Chapter 5

Modelling Sea Level Rise from Ice Sheet Melting in a Warming Climate

Diandong Ren, Lance M. Leslie and Mervyn J. Lynch

Additional information is available at the end of the chapter

http://dx.doi.org/10.5772/55529

1. Introduction

Sea level change can arise from fluctuations in ocean basin size and/or water volume. The fluctuations can have many causes, including filling from landslides; water from melting of ice sheets and mountain glaciers; steric water expansion from temperature increases; seabed deformation; and extended dry or wet periods. Here, the focus is on model projections of sea level rise (SLR) from ice sheet melting in a warming climate. The modelling system is SEGMENT [1,2], which embraces a range of geophysical flows, has a modular design and supports multi-rheology flows. For ice-sheet modelling, the SEGMENT-Ice module incorporates the complexities of both internal flow, and interactions of the ice sheet with its external environment at its upper and lower boundaries, and along its perimeter. Recent applications of SEGMENT-Ice to the Greenland Ice Sheet (GrIS) and the Antarctic Ice Sheet (AIS) show that it simulates well the ice flow patterns in a variety of different spatial configurations, such as slow moving sheet ice, fast moving stream ice, and shelf ice. It also accurately represents many characteristics of the ice sheets, such as internal deformation, basal sliding, ice shelf calving, and temperature profiles within ice.

Quantifying SLR is a major challenge. Two main factors have contributed to the observed global SLR. One factor is the increased melting of land-based ice. The major sources of stored water on land are ice sheets, polar ice caps and glaciers. The other factor is the thermal expansion of the oceans, as warming ocean water expands. A potential third factor, also related to a warming climate, is the greater filling of the sea basin from landslides and soil erosion. The present melting of land ice is comparable with ocean thermal expansion. In a future warming climate, melting is expected to increase. For example, the melting of the GrIS has been identified as a critical, but poorly understood, process in determining global SLR in the 21st century. The Intergovernmental Panel on Climate Change (IPCC) has estimated the GrIS

contribution to be ~24 mm by 2100, compared with 1990 levels. This is regarded as an underestimate, as recent observations indicate that peripheral outlet glaciers are highly sensitive to atmospheric warming. Observational and modelling studies of mass loss from ice sheets, glaciers and the polar ice caps indicate a contribution to SLR of ~0.2 to 0.4 mm/yr averaged over the 20th century. Globally averaged SLR was at a rate of ~1.7 ± 0.3 mm per year over 1950 to 2009 and at a satellite-measured average rate of ~3.3 ± 0.4 mm per year from 1993 to 2009, a marked increase over earlier estimates.

This chapter projects the sea level contribution from ice sheets through to 2100, using SEGMENT-Ice forced by atmospheric parameters derived from three different climate models (CGCMs). Notably, SLR contributions from AIS, its increased discharge (indicated by increased ice flow and calving rate) and another previously overlooked factor (the change of West Antarctic Ice Sheet (WAIS) basin size as WAIS disintegrates), are presented. In 2007, the IPCC AR4 projected that during the 21st century, sea level will rise another 18 to 59 cm, but the IPCC projections include neither "uncertainties in climate-carbon cycle feedbacks nor the full effects of changes in ice sheet flow" [3].

2. Sea level rise from melting of the cryosphere in a warmer climate

The IPCC estimate of 21st Century excluded “future rapid dynamical changes in ice flow.” This caveat was added as no ice sheet model had reproduced observations of ice sheet elevation and velocity changes. Calculating the evolution of these changes was not yet possible. Observed rapid changes have several causes. These include penetration of surface melt water to the ice-sheet bed, enhancing acceleration of ice flow [4,5]; sudden disintegration of floating ice shelves with ensuing acceleration of glaciers flowing into the now-removed ice shelf area [6,7]; and penetration of warm water beneath floating ice shelves, causing significant reductions in the buttressing effects of ice on larger outlet glaciers feeding floating ice shelves [8]. Early attempts to model these processes show large possible losses of ice [9,10,2]. The difficulties in projecting future sea level change encouraged the glaciology community to understand the causes of observed changes, and in a deterministic way such that causal processes are included in numerical predictive ice sheet models. Workshops discussed the required process studies, and the means to improve the skill of existing ice-sheet models [11-13]. It became clear that new field studies of key processes were necessary, along with improved numerical models of ice sheet flow incorporating both a better representation of fast flowing ice, and the processes driving rapid responses of ice sheets. SEGMENT-Ice is one model implementing these improvements and is showing encouraging predictive skill by incorporating new processes such as granular basal sliding (e.g. till rheology in the dynamics of tidewater glaciers), tabular calving and grounding line dynamics. Model results described here are intended to improve upon the present relatively limited value of sea-level projections in the previous IPCC report.

http://dx.doi.org/10.5772/55529

2.1. Regional sea level rise contributions from the Greenland Ice Sheet

This section projects the SLR from the GrIS through to 2100, using SEGMENT-Ice forced by atmospheric parameters derived from three coupled global climate models (CGCMs). The geographical patterns of near-surface ice warming impose a divergent flow field favoring mass loss through enhanced ice flow. The average model mass loss rate during the latter half of the 21st Century is ~0.64±0.06 mm/year eustatic SLR, significantly larger than the IPCC estimate from surface mass balance. The difference is due largely to positive feedbacks from reduced ice viscosity and the basal sliding mechanism present in the ice dynamics model. This inter-model, inter-scenario spread adds ~20% uncertainty to ice model estimates. The SLR is geographically non-uniform and reaches 1.69±0.24 mm/year by 2100 for the northeast coastal region of the United States, amplified by a weakening of the Atlantic meridional overturning current (AMOC). In contrast to previous estimates, which neglected the GrIS fresh water input, both sides of the North Atlantic Gyre are projected to experience SLR. Impacts on major cities on both sides of the Atlantic, and in the Pacific and Southern Oceans, are assessed. The Atlantic Ocean cities are the most affected. Land ice melting likely will increase in a warming climate [14]. The IPCC estimates the SLR contribution from the GrIS will be 24 mm by 2100, compared with 1990 levels. This likely is an underestimate, as during the past decade the large mass loss (reaching ~0.7 mm/yr sea level contribution in 2010) likely is the result of climate warming. The warming has lasted long enough for the already accumulated effects to be irreversible by just several events, such as one or two years of cooler than annual mean temperatures. For example, the 2010 Iceland volcanic eruption did not slow the melting rate. The SEGMENT-Ice GrIS modeling study described here attempts to reduce the uncertainty in quantifying the global SLR from the GrIS, and to explore its regional manifestations. SEGMENT-Ice has a detailed, enhanced treatment of basal and lateral boundary conditions and 'higher order' terms [1]. SEGMENT-Ice was compared with other models in the SeaRISE project, and showed encouraging skill in reproducing and explaining recent, dramatic ice sheet behavior [15,16].

2.1.1. The ice model

SEGMENT-Ice is a component of an integrated scalable and extensible geo-fluid model (SEGMENT). It solves the conservation equations for mass, momentum and energy for the simulation domain, under the rheological relationships of the participating materials. The energy is bundled in a convenient form for considering phase changes and formation of new interfaces (e.g. Griffith cracks and von Mises yielding conditions). In this subsection, the focus is on the GrIS (Fig.1). Parameterization of viscosity is critical for ice creeping. SEGMENT-Ice has two improvements over Glen's ice rheological law, for factoring in flow induced anisotropy, and granular basal condition. Flow enhancement by re-fabricating [17] is implemented so that older ice, farther from the Summit, is easier to deform. SEGMENT-Ice also allows a lubricating layer of basal sediments between the ice and bedrock, which enhances ice flow and forms a positive feedback for mass loss in a warming climate [18,19,1]. Because the ocean temperature is higher than around Antarctica, Greenland has no ice shelves. There however are several water-terminating fast glaciers around the peripheral of GrIS, such as Jakobshavn (J), Kangerdlugssuaq (K), Helheim (H), and Petermann (P) glaciers. In SEGMENT-Ice, ocean-

ice interactions are parameterized, with freezing point depression by soluble substances, salinity dependence of ocean water thermal properties, and ocean current-dependent sensible heat fluxes included.

As the climate warms, increased air temperature through turbulent sensible heat flux exchange increases surface melting and runoff. Similarly, changes in precipitation affect the upper boundary input to the ice sheet system. For the 200-year period of interest here, major ice temperature fluctuations are near the upper surface of the GrIS. The strain rate, however, can be large near the bottom and/or the surface, so SEGMENT-Ice has a 31 vertical level, stretched grid to better differentiate the bottom and near surface. The uppermost layer is 0.45 m thick near the GrIS Summit, fine enough to simulate the upper surface energy state on a monthly time scale. Because of its location, the GrIS is an important contributor to eustatic SLR, ocean salinity and the North Atlantic thermohaline circulation [20] In SEGMENT-Ice the total mass loss comprises surface mass balance and the dynamic mass balance due to ice flow divergence. Total mass balance is converted to water volume and is used here as a proxy for the eustatic SLR contribution.

In ice flow, inertial and viscous terms counteract pressure gradient forces. The full Navier-Stokes equations are used in the momentum equations of SEGMENT-Ice. Because of comparably large aspect ratios, ice streams and surrounding transition zones are the areas where a full Stokes model is needed most [21]. SEGMENT-Ice uses a terrain following coordinate system, the sigma coordinate system, σ (grid lines in inset of Fig. 2), defined as $\sigma = (h - r)/H$, where h is the distance from the ice surface to the Earth's centre and H is the local ice thickness, and r is the independent variable in the radial direction in the spherical coordinate system. A vertical integration of the incompressible continuity equation, with surface mass balance rate and basal melt rate as boundary conditions, gives:

$$\frac{\partial h}{\partial t} = - \frac{1}{R\cos\phi}\int_0^1 \left(\frac{\partial u}{\partial \theta} + \frac{\partial v\cos\phi}{\partial \phi}\right) H ds - \frac{u_s}{R\cos\phi}\frac{\partial h}{\partial \theta} - \frac{v_s}{R}\frac{\partial h}{\partial \theta} - w_b + b \quad (1)$$

where t is time, R is the Earth's radius, θ is longitude, ϕ is latitude, u and v are the horizontal velocity components, and w is the vertical velocity component, which is expanded using the continuity equation, assuming incompressible ice. The subscripts 'b' and 's' mean evaluated at the bottom and upper ice surfaces. Equation (1) diagnoses the temporal evolution of the surface elevation, which also is the ice thickness because bedrock is assumed unchanged over a time scale of several hundred years. The surface elevation varies as a function of velocity fields and boundary sources. The surface mass balance rate, b, also includes basal melt rate. For the AIS, it primarily is the net snowfall (precipitation less sublimation and wind redistribution) minus basal melting, in ice thickness equivalent. The change in ice thickness multiplied by grid area is the volume ice loss for that grid. The total ice loss is the summation over the entire simulation domain. In Eq. (1), the first term on the right hand side is the vertical velocity, w, evaluated at the upper ice surface.

http://dx.doi.org/10.5772/55529

2.1.2. Input and verification data

SEGMENT-Ice requires initial conditions and static inputs, such as ice thickness, free surface elevation, and the three-dimensional ice temperature field at the initial time of integration, obtained from the SeaRISE project (http://websrv.cs.umt.edu/isis/index.php), at 5 km horizontal resolution. The bottom geothermal distribution is assumed constant over the 200-year simulation. The SLR contribution from the GrIS is from the total mass balance: i.e. input (e.g., snow precipitation, flow convergence) minus output (e.g., surface melt water runoff, flow divergence to open waters or calving). Atmospheric temperature, precipitation and near surface radiative energy fluxes all are critical factors for the future total GrIS mass balance. The CGCMs provide the meteorological forcing. The large natural variability justifies using extended atmospheric time series to extract first-order feedback GrIS signals in a warming climate. The three independent CGCMs (MPI-ECHAM, NCAR CCSM3 and MIROC3.2-hires (see http://www-pcmdi.llnl.gov/ipcc/about_ipcc.php) are chosen for their relatively fine resolution and for providing all atmospheric parameters required by SEGMENT-Ice. Their projections of precipitation and temperature, two key factors affecting ice-sheet mass balance, produce a large spread in the multi-model assessments [3] by 2100.

In addition to atmospheric parameters, to investigate the ice ocean interactions at the water terminating glaciers (e.g., Jacobhavn, Kangerdlugssuaq, Petermann and Helheim), additional variables such as the ocean flow speed, potential temperature, salinity, and density are needed. Density is dependent as it is a function of temperature, salinity and pressure. For outlet glaciers north of 70°N, CGCM ocean model output at 0, 10, 20, 30, 50, 75 and 100 m depths are interpolated to SEGMENT-ice grids. For the Helheim glacier, which resides in the Sermilik fjord, the 1-km resolution, ice thickness data from SeaRISE indicates a terminus depth of about 700 m, close to the estimate of [22]. Oceanic parameters up to 1000 m are used for this glacier. The University of Hawaii data (http://uhslc.soest.hawaii.edu/jasl.html) are used to evaluate projections of regional SLRs.

2.1.3. Sea level contribution from additional melting of the Greenland Ice Sheet

SEGMENT-Ice is integrated forward in time with climate model meteorological forcing over the GrIS, to provide the total mass loss trend over the 21st Century. Monthly atmospheric forcing and the advanced numerics of SEGMENT-Ice can in principle produce realistic monthly fluctuations in ice sheet properties. However, interannual and decadal climate variations in CGCMs largely are random noise, as are ice model projected quantities on the same time scales. Thus, no attempt is made to compare them with *in situ* observations of the model projections on inter-annual to decadal scales. Monthly SEGMENT-Ice output is averaged to obtain annual mean values. A 21-point binomial smoother is applied to the annual means to remove short-term variability. The smoothed lines in Fig. 2 show the eustatic SLR contribution from the GrIS for the 20th and 21st Centuries. For each model, the atmospheric forcing is under the three non-mitigated IPCC Special Report on Emission Scenarios (SRESs): B1 (low); A1B (medium); and A2 (high rate of emission). Total ice volume is a highly aggregated metric and the trend is the resultant of several factors. As inland GrIS remains cold, the feedback from increased precipitation (see Fig.3b) is significant. Therefore, estimates of the

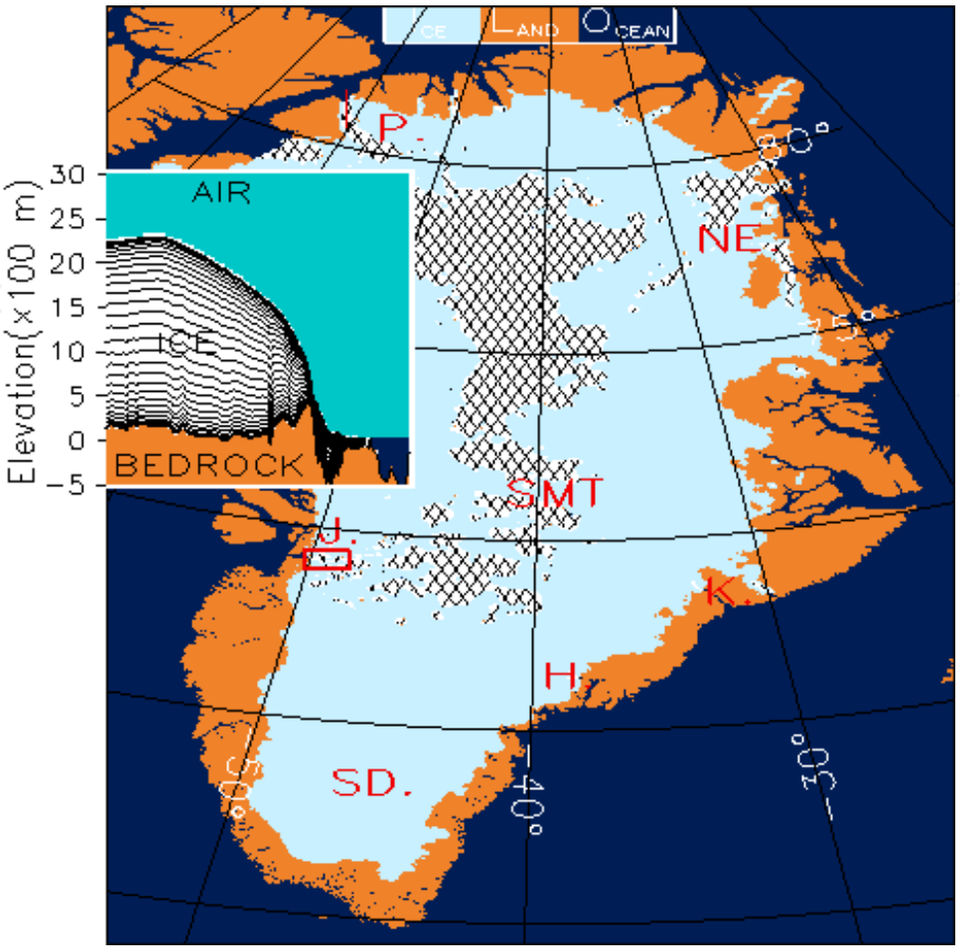

Figure 1. The Greenland Ice Sheet and land cover mask. "L" is land, "O" is ocean. The locations of the Jakobshavn (J.), Kangerdlugssuaq (K.), Petermann (P.) and Helheim (H.) Glaciers, and the North East (NE) ice stream are labelled. Hatched areas are regions with ice loads but with bottom elevations lower than the present sea level. The inset is a zoomed Petermann glacier showing a vertical cross-section.

GrIS contribution to SLR are less sensitive to scenario assumptions before 2030, despite atmospheric forcing diverging after year 2000. After 2030, as atmospheric forcing diverges further, the differences become clear.

The total mass balance terms indicate that the higher precipitation amounts (mm/day) from strong scenario B1 (Fig. 3b) eventually are dominated by increased ice flow divergence and surface melt-water runoff from higher near surface surface temperatures (Fig. 3a). After 2060, the mass loss rate accelerates, as basal sliding becomes significant, especially below the southern tip and the northeast ice stream, signifying a faster mass shed [19]. For the GrIS, the positive feedback from strain heating and reduced ice viscosity may have longer time scales. The consensus is weak scenario B1 has far less total mass loss than the A2 and A1B scenarios, by the late 21st Century.

Sea surface elevation is maintained by atmospheric parameters, and is sensitive to climate changes and it produces corresponding regional sea level adjustments. In addition to factors affecting global SLR, the geographical distribution of SLR adds further complexity, being

http://dx.doi.org/10.5772/55529

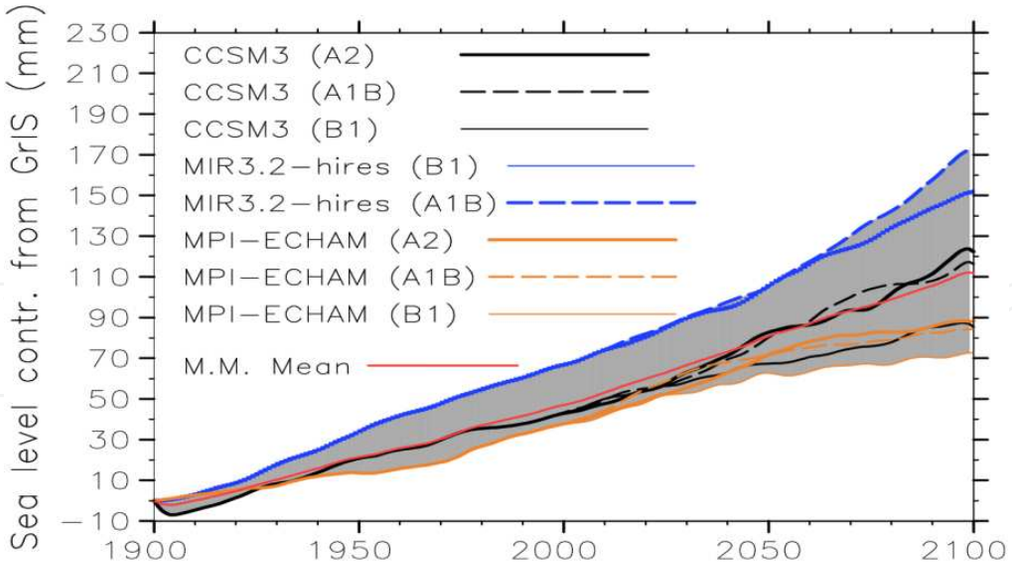

Figure 2. Eustatic SLR (mm) from the GrIS for 20th and 21st centuries, forced by. CCSM3, MPI-ECHAM and MIROC3.2-hires climate models under IPCC scenarios SRES A2, A1B and B1. Red curve is the multi-model multi-scenario mean. Colour shading is model spread.

affected by changes in flow divergence/convergence from ocean currents [23]. For example, owing to the Coriolis force associated with the Gulf Stream, the regional sea surface along the east coast of the United States has a slope tilting seaward. Fresh water discharge from the GrIS weakens the AMOC, suggesting a dynamic adjustment of sea surface elevation. For northeast coastal United States, this produces an additional SLR superimposed on the eustatic SLR. All CGCMs show the largest sea level rebound in the southern Labrador Sea. However, the southern oceans are quite different. With the future strengthening of the Antarctic circumpolar circulation (ACC), the ocean surface slope maintained by the Coriolis force increases, with a significant SLR over an ocean belt at ~46 degree south. The mean change for 2091–2100, relative to 1981–2000, projected by three AR4 climate models under the A1B scenario, reaches 0.4 m over a 10^5 km^2 area of the southern Indian Ocean. A similar, smaller pattern occurs along the east coast of South America. Contributions to SLR from GrIS melting were calculated for 8 coastal cities, calculated from sea level changes with and without GrIS water routing. Southern Hemisphere cities, Cape Town and Sao Paulo, are selected for their proximity to western boundary retroflection currents. Unlike eustatic sea level change, which is approximated empirically [14], quantifying the geographic manifestation of the 0.64 mm/yr global mean SLR requires the inclusion of ocean currents. A CCSM3 sensitivity experiment identified regional GrIS contributions to SLR. The three major contributors: steric, melt water input and ocean dynamics are interconnected; a CGCM is needed to assess the effects of fresh water input. For each scenario, there is monthly forcing from 1900 into the Atlantic Ocean.

The GrIS net mass loss rate matches the time series in Fig. 4 but uses the geographical routing pattern from the ice model. Fig. 4 shows the geographic significance of the SLR, with the sea level time series for three Northern Hemisphere coastal cities: London, New York and San Francisco. Ensemble means of projected sea level change series from CCSM3 after 1900 and

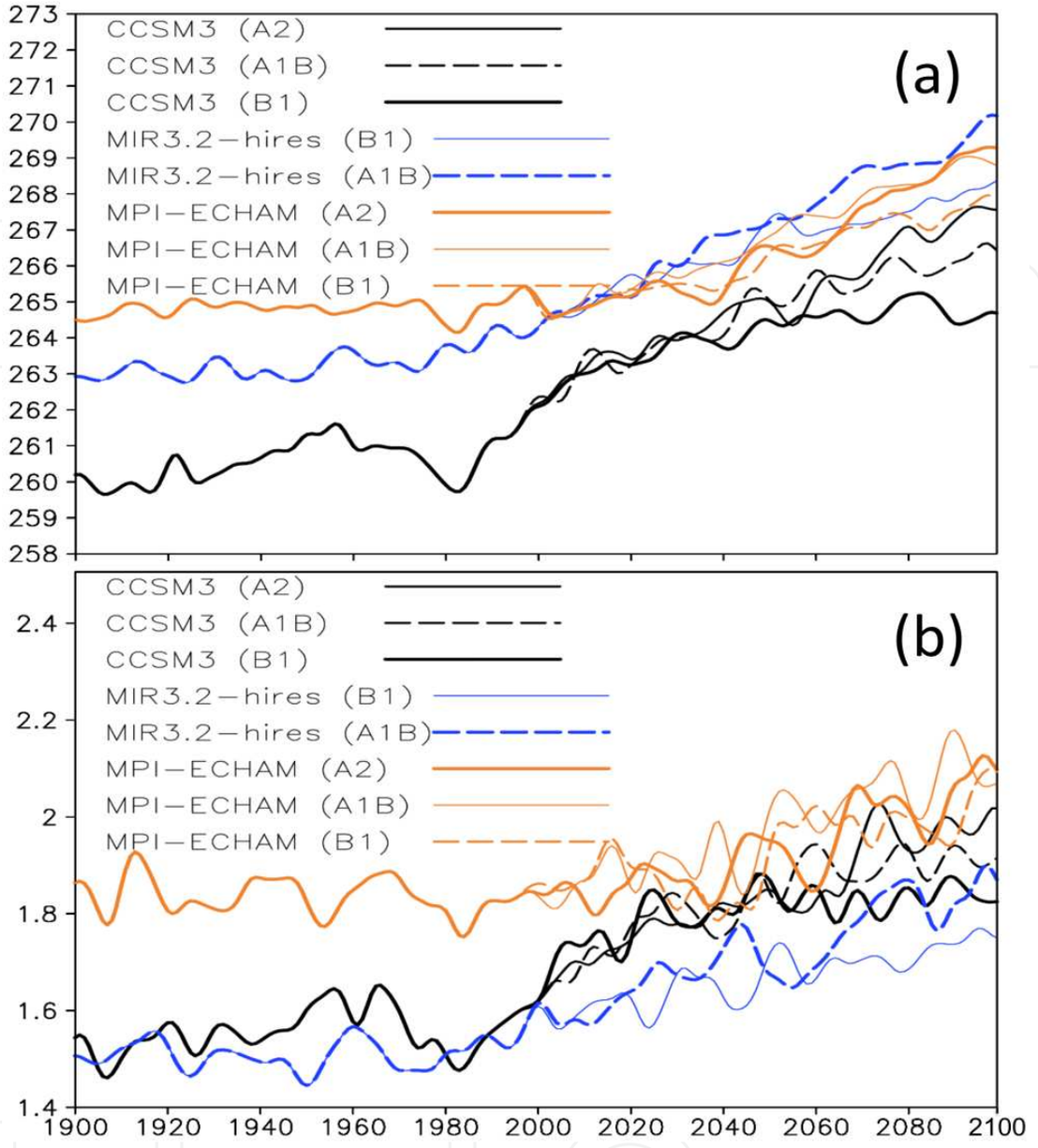

Figure 3. Time series are shown of the 21 point (20 year) low-pass filtered mean near surface temperature (°K, Panel a) and precipitation (mm/day, Panel b) over Greenland, from three climate model simulations with different anthropogenic forcing scenarios. The SRES A2 simulation is not available for the MIR3.2-hires climate model at the time of writing.

expected ensemble mean CGCM projections, neglecting GrIS contributions are compared. The CCSM3 rates are lower than observations (see Fig. 5, which has 8 cities). At 99.5% confidence interval, linear trends for observed and modelled SLRs are: 1.77±0.35 and -0.13±0.7 mm/yr for London; 1.84±0.51 and 0.05±0.1mm/yr for San Francisco; and 2.64±3.05 and 0.31±0.67 mm/yr for New York. GrIS melting reduces the underestimation, especially for Atlantic Ocean cities (1.16±0.7 for New York and 0.47±1.0 mm/yr for London). The greatest rise, for New York City, is from 0.31 to 1.16 mm/yr and is 1/3 closer to reality. For the latter half of this century, the global 0.64 mm/yr SLR increases to ~1.69 mm/year near New York. Fresh water from the GrIS

http://dx.doi.org/10.5772/55529

contributes most to SLR northwest of the north Atlantic gyre, with greater impact on cities like New York City. For ocean dynamic adjustment, alone, the London SLR slows then ceases after 2050 as water mass is redistributed to the west coast of the Atlantic Ocean, adapting to a reduced Coriolis force. However, fresh GrIS water causes SLR near London.

In contrast, GrIS melt water is not a major SLR contributor in the Pacific Ocean (e.g., San Francisco, Fig. 5 below) and in the southern oceans (e.g., Sao Paulo) where dynamic sea level adjustments are significant but the GrIS contribution is small.

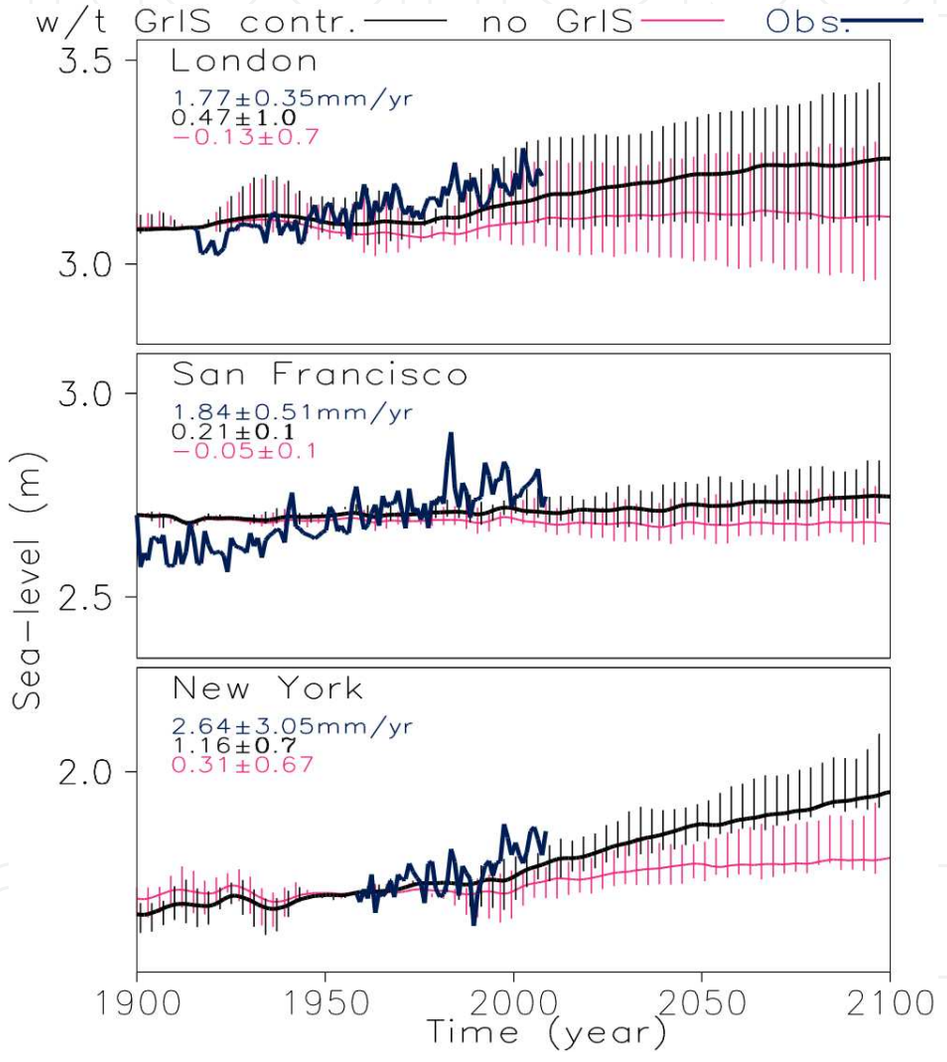

Figure 4. CCSM3 simulated sea level evolution during 1900-2100. Model simulations are performed under the corresponding scenario run but with fresh water routing from the GrIS. The thick, 20-year smoothed black (red) curves are ensemble mean of the multiple model runs with (without) fresh water routing from the GrIS. Vertical bars are the upper and lower envelopes. Blue lines are from tide gauge observations (UHSLC research quality sea level station data). Climate model predictions are shifted so observed and modelled values match at the first observational data grid. The trends and uncertainty range (p=0.05) over the observational period are also given. In generating the fresh water routing scenario, SEGMENT-Ice is forced by CGCMs under different scenarios. For melting fraction of water, the routing scheme of the existing river transport model is used, close to the basin division in [24]. Calving ice is transformed into sea ice fraction with zero salinity.

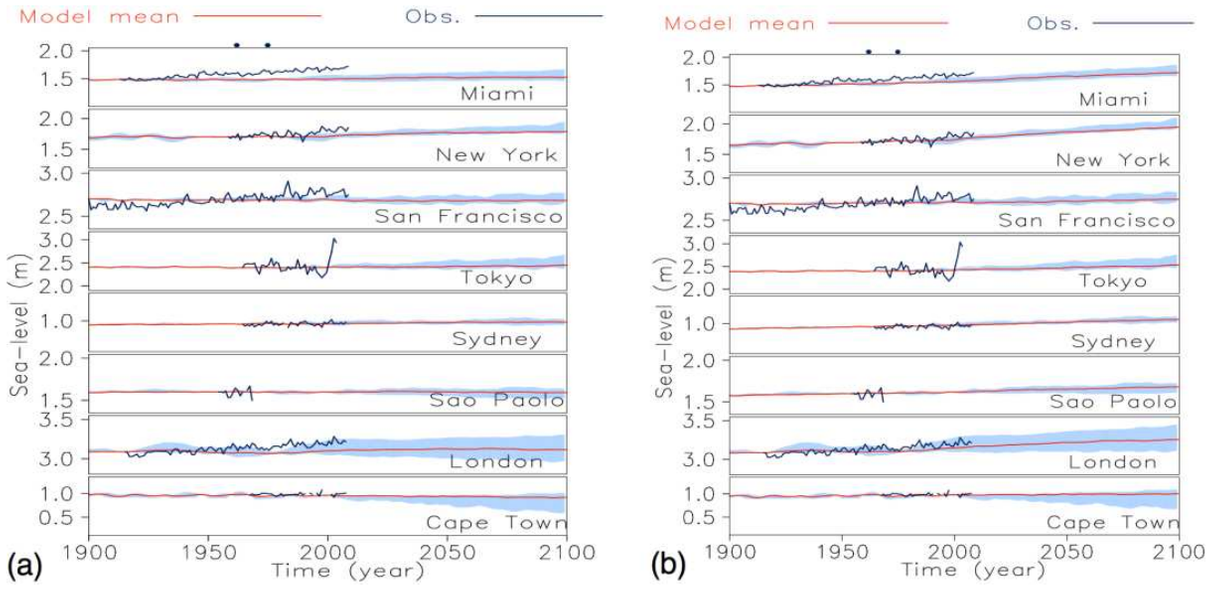

Figure 5. Regional sea level rises near 8 global cities. (a) Without Greenland Ice Sheet fresh water contribution. (b) With Greenland Ice Sheet fresh water discharge

2.2. Eustatic sea level rise contributions from the Antarctic Ice Sheet (AIS)

In this section, the same SEGMENT-Ice system is used as in the previous subsection. However, because of the more complex bedrock-sea water-until configuration, and the increased prevalence of ice shelves, parameterizations that are more physical are activated in the simulations. To minimize the uncertainties associated with the basal granular material, remotely sensed surface velocities are used to deduce the basal mechanical properties and substrata depth [2]. The following is a concise description of the tabular calving scheme and the grounding line dynamics in the SEGMENT-Ice model, and a context is provided for the mass loss and sea level contributions.

2.2.1. An ice shelf approximated by a cantilever beam

An ice sheet is composed of fast-moving, channelized ice streams that drain thick, slower-moving inland ice. Due to the present relatively cold ocean temperatures around the AIS, inland ice streams discharge into the ice shelves, which are the floating extensions of the AIS. The ice shelf mechanics component of SEGMENT-Ice is not available for previous GrIS studies. The ice shelf parameterization in SEGMENT-Ice is derived from an ice shelf's life cycle, which is an advancing-thinning-attrition cycle (Fig. 6). Ice is brittle at higher strain rates, especially under tension, with a melting point diffusivity ~10^{-15} m^2/s, much lower than that for elemental metals. For inland ice, crevasses/cracks collocate with locations of concentrated strain rates, for example, after ice flows from relatively gentle into much steeper bedrock slopes (Fig. 6), which is the case for the Pine Island Glacier of the West Antarctic Ice Sheet (WAIS). At the flanks of ice stream, crevasses caused by transverse strain also are prevalent. When ice crosses the grounding line and floats, its contribution to SLR is negligible. Nevertheless, ice shelves

http://dx.doi.org/10.5772/55529

are integral components of an ice sheet's thermo-dynamic system. For example, the discharge rate of inland ice is influenced by the buttressing restraint provided by the ice shelves [25].

The following is a flow-dependent ice shelf calving scheme unique to SEGMENT-Ice. Figure 7 illustrates the calving physics implemented in SEGMENT-Ice. The shelf is in near hydrostatic balance with the ocean waters, but the flow structure inside the ice-shelf determines that it is a dynamic scenario of advancing-thinning-breaking, from grounding line toward the calving front. In Fig.6, upper panel (a) is a conceptualization of the Amery Ice Shelf. Compared with land ice, where shear resistance counters most of the surface elevation caused by gravitational driving, ice shelves thin by creep thinning.

Except at the very bottom, the cryostatic pressure inside the ice always is higher than the hydrostatic pressure at the same level from the ocean water. The differences (net horizontal stress) reach a maximum at sea level (the thin red curve in Fig. 6a). Hence, the vertical variation of horizontal shear and the vertical profile of the velocity have a turning point at sea level. The negative vertical strain rate (compression) causes a horizontal divergent (positive) strain rate. Inside the ice shelf, the spreading tendency is restrained mainly by along flow stress. Ice shelves spread under their own weight and the imbalance pushes most at the calving front and around the grounding line. According to [26], this horizontal compression produces an anvil shaped outreach at the calving front [27, 28]. The forward slanting of the Amery Ice Shelf at the calving front (Fig. 6c) is a manifestation of the vertical shear in the ice flow. As shown in Fig.7, although the bulk of the shelf is in hydrostatic balance with the ocean water, the "mushroom" shaped, girder-like spread section usually is not. The limiting length of this portion, before breaking from the main body of the shelf (b_k in the diagram), is limited by the tensile strength of ice (~2 Mpa at present for marginal regions of the Ross Ice Shelf), the ice thickness (H) and the ice creeping speed and vertical shear. In general, the tensile strength of ice can vary over a wide range depending on temperature, strain rate and grain size, as natural ice is polycrystalline. This length is regularly approached, causing systematic calving of an ice shelf. There are random components in the calving processes, such as hydro-fracturing [29], which produce ice shelf lobes. Based on elastic mechanics and a cantilever beam approximation, it is proposed that:

$$b_k = \left[\frac{f D_T H}{\left(3\rho_i g \left(1 - \frac{C_T \rho_i}{\rho_w}\right)\right)} \right]^{0.5} \quad (2)$$

where $\rho_w = 1028\ kg\ m^{-3}$ is the density of sea water, ρ_i is the density of ice, g is gravitational acceleration, C_T is a factor taking tidal and sea wind swelling into consideration, and D_T is a dimensionless factor measuring the ratio of Ice flow shear to surface ice velocity. D_T is a function of ice temperature. The density of ice varies with loading pressure. Ice density is sensitive to overloading because the ice has air bubbles encapsulated during the transition from snow to firn and further into glacial ice. Below, a more rigorous derivation is provided of Eq. (2), based on a cantilever beam approximation. Most AIS peripheral ice shelves are cold, with little surface melting year round, so the tabular calving largely is by gravity cracking. As the shelf falls, the buoyancy increases quickly, so it is rare that a complete cut results from a

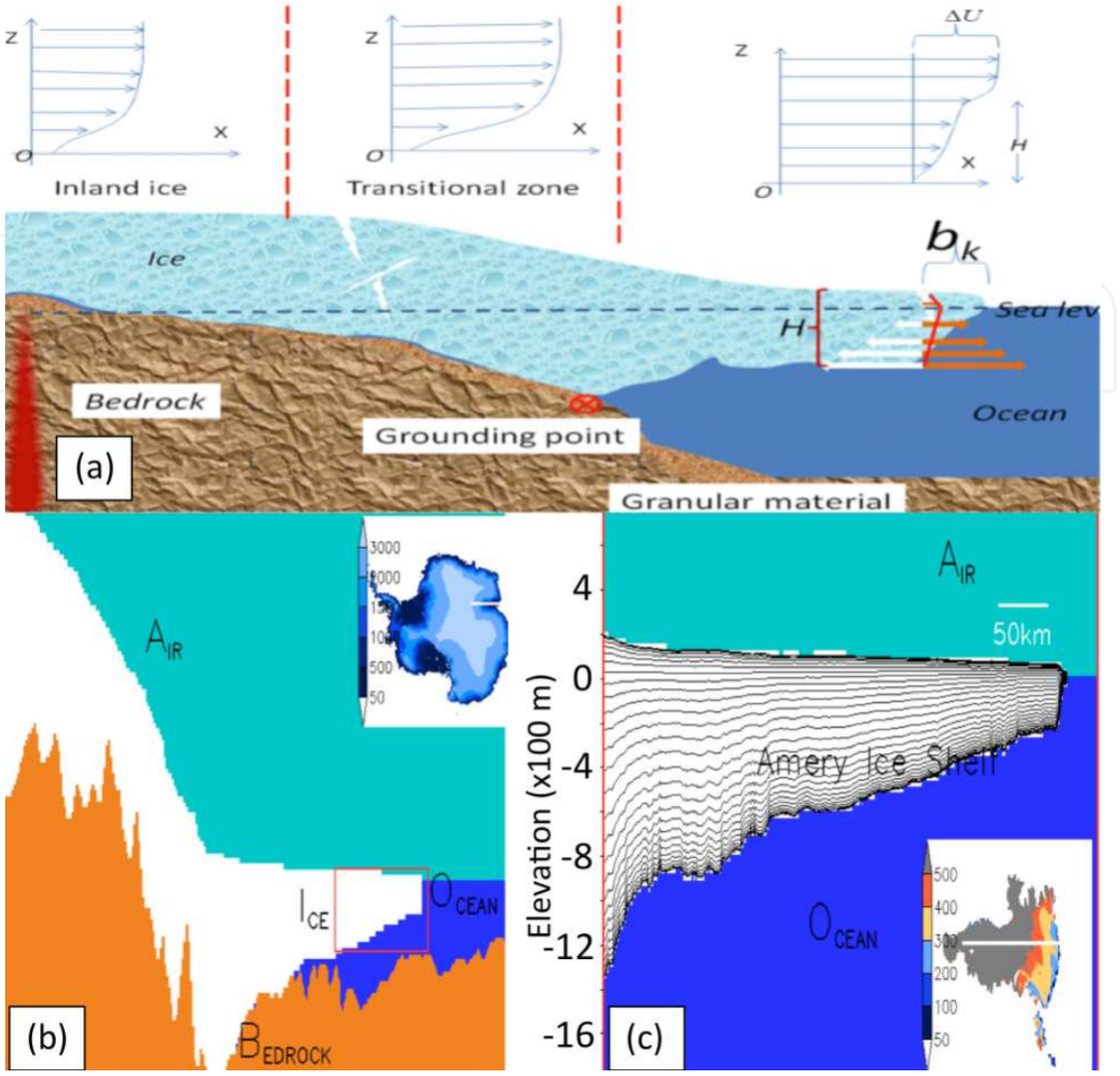

Figure 6. Ice-shelf calving in SEGMENT-Ice. The upper panels in (a) are schematic diagrams of ice profiles, showing the different flow regimes. Note that, due to granular material, the basal velocity is not exactly zero. The acceleration of the ice (to the right) causes the ice to be torn. Inside the ice-shelf, the spreading tendency is restrained mainly by longitudinal stretching (along flow stress). Ice shelves thin by creep thinning. The negative vertical strain rate (compression) causes a horizontal divergent (positive) strain rate. The ice shelf's velocity increases toward the calving front as determined by the spatial integral of the horizontal strain rate. In the diagram, white bulk arrows are stress (hydrostatic pressure) on the right side of the calving front exerted by the ocean, decreasing to zero at sea level. Red bold arrows are static stresses exerted on the left side of the front, decreasing linearly to zero at ice upper/sub-aerial surface. At the shelf bottom, hydrostatic stresses from both sides are almost equal. Red curve is the net horizontal stress, which reaches a maximum at sea level. Hence, vertical variation of horizontal shear and the vertical profile of the velocity have turning points at sea level. The diagram is partially adapted from T. Hughes via R. Bindschadler (personal communication 2011). The vertical profile of the horizontal ice velocity field determines that there will be a "mushroom" shaped spread section not in hydrostatic balance with the ocean water, unlike most of the shelf section. There is a limit to the length of this section before it breaks off from the main body of the shelf (b_k in the diagram). Panel (b) is a cross section of the Amery Ice Shelf (5km DEMs are used in the plotting, indicated in the inset white dashed line). (c) is a zoom-in of the red line confined region in (b), with 1-km resolution ice thickness and surface elevation maps, to illustrate the forward slanting of the calving front. Inset colour shadings are ice thicknesses.

single crack. Periodic forcing from waves and random collision with sea ice and icebergs usually follows fatigue. To generalize these processes and express them as a numerical

http://dx.doi.org/10.5772/55529

algorithm, a cantilever beam approximation is used to estimate the calving frequency. As shown in Fig. 7, it is assumed that the material is stiff and the deflection in the *z*-direction is sufficiently small that linear deformation theory for elastic material is valid. It further is assumed that the cross-section is rectangular to remove variations in the *y*-direction and work only in the *x*-*z* plane (the convention for moment and torque are all in a right-handed coordinate system, as in Fig. 7. The beam material has an elastic modulus E and density ρ.

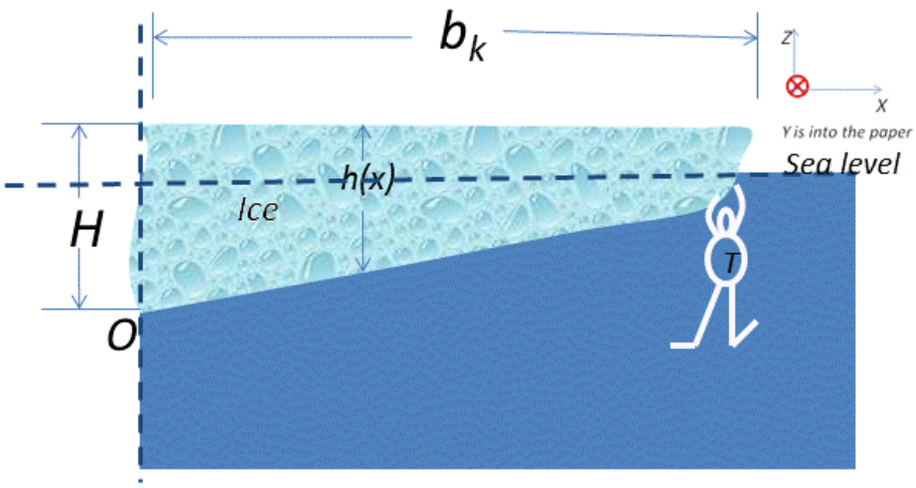

Figure 7. Cantilever beam assumption for an ice shelf. *H* is the ice thickness at the hanging side, which is connected with the main shelf. The *y*-*z* cross section is assumed rectangular, and ice thickness *h(x)* is assumed linear. *T* denotes external loading, such as tides or random collisions with other icebergs. Small deflections in the z-direction are assumed.

As the cross-section is assumed rectangular, the area moment of inertia is $I = H^3/12$ at O. The momentum around O exerted by the weight of the beam and an external loading (tides and other random factors), T, at the tip end of the shelf is expressed as:

$$M = \int_0^{b_k} x\rho g h\,(x)dx + T\,b_k \tag{3}$$

where g is gravitational acceleration (9.8m/s^2), and M is the moment in the positive y direction. In a static state, the resistance moment should in the *negative* y-direction and of the same magnitude. Because of moment drive, there is potential energy stored around the cross-section passing through O:

$$W = 2EI\,/\,Hr \tag{4}$$

where r is the curvature of the beam at O. At the yielding condition, $f_c = E/r$ is the tensile strength of ice. In Eq. (4), the factor of 2 appears because mass conservation is assumed, so that the cross-sectional area experiencing compression and the area experiencing expansion are the same. The relation between strain and Young's modulus are applied, producing the factor of 2. The stored potential energy and the moment should have the same value. That is:

$$2 f_c I = HM \tag{5}$$

Equation (5) is the key equation for obtaining the limiting length of ice shelf before attrition. For example, if we assume the linear ice thickness profile:

$$h(x) = H - kx \tag{6}$$

where $k = \frac{H}{b_k}\frac{\rho_i}{\rho_w}$

where ρ_w and ρ_i are respectively the density of water and ice, then substituting into Eqs. (3) and (4), and using Eq. (5), gives:

$$b_k = \frac{-3T}{2a} + \left(\frac{9T^2}{4a^2} + \frac{c}{a}\right)^{0.5} \tag{7}$$

where $a = \rho_i g H\left(1 - \frac{\rho_i}{\rho_w}\right)$, and $c = -\frac{1}{2} f_c H^2$. For the case without external loading, $b_k = \left[f_c H \Big/ \left(2\rho_i g\left(1 - \frac{\rho_i}{\rho_w}\right)\right)\right]$. This is similar to Eq. (2). In Eq. (2), a more realistic ice profile was assumed in reference to ice flow vertical shear and the further assumption of Eq. (7) was made of assuming T is small compared with the integral part of Eq. (3) (the first term on the right hand side). Ice shelf calving in essentially a fatigue process of visco-plastic ice. In SEGMENT-Ice, the von Mises yielding criteria (a critical point for ice to deform plastically) is applied to identify initial seminal crevasses for inland ice. In principal deviatoric stress form:

$$\sigma_f = \left[\frac{3}{2}\sum_{i=1}^{3}(\sigma_i)^2\right]^{0.5} \approx 100 Mpa \tag{8}$$

As different parts of the ice-shelf calving front have different ice thicknesses and speeds, it is unlikely a complete cut occurs at once. The typical scenario is that one sector breaks first, and the crack propagates laterally to the neighbouring area. Tides and other random oscillating factors play a role in the speed of the crack, because a crack that does not cyclically open and close does not grow rapidly. Tidal amplitudes around Antarctica generally are small compared with ice thickness except for the portion facing South America. Only those tides with the resonance frequencies of the ice shelves have significant effects on the crack tearing rates. In SEGMENT-Ice, the crack tearing rate is expressed as

http://dx.doi.org/10.5772/55529

$$\frac{da}{dN} = c_1 e^{C_0|\upsilon-\upsilon_0|}(\Delta K)^4 \quad (9)$$

Where a is the crack length starting from 0, N is time steps, c_1 is the Paris coefficient [30], C_0 is a negative number indicating the exponential damping of the tidal tearing when it is out of synchronization with the natural frequency of the ice-shelf, υ is the tidal frequency and υ_0 is resonance frequency of the ice shelf under consideration, and is ΔK the range of stress intensity change (proportional to square of the amplitude of the tide). The resonance frequencies are determined for all peripheral ice shelves.

2.2.2. Grounding line dynamics

In SEGMENT-Ice, ocean-ice interactions are parameterized so that freezing point depression by soluble substances, salinity dependence of ocean water thermal properties, and ocean current-dependent sensible heat fluxes are included. SEGMENT-Ice has a chemical potential sub-model to estimate the effects of ocean water salinity changes on the grounding line retreat of water terminating glaciers and erosion of ice shelves. SEGMENT-Ice uses a molar Gibbs free energy bundle in considering phase changes. Melting/refreezing is determined by the chemical potential of H_2O in both states, across the interface. SEGMENT-Ice estimates ice temperature variations then it calculates the fraction of melted ice. When the terminal heat source becomes a heat sink, freezing occurs and ice extends beyond the initial interface, simulating the grounding line advance/retreat. When newly formed ice is less than the dimension of the grid mesh, it records the fraction that melts first when the heat flux reverses. If newly formed ice fills a grid box, SEGMENT-Ice adjusts its "phase-mask" array, to indicate the new water/ice interface. Melting is analogous.

2.2.3. Mass balance and sea level contribution

The simulated present 3D ice flow field, using the retrieved granular properties, current ice geometry, and current climate conditions (Figures not shown), agrees well with InSAR measurements and provides more information than the InSAR measurements. For example, from the Modified Antarctic Mapping Mission (MAMM, [32]), the Ross Ice Shelf has a large downstream flow speed. The model shows that for most of the flat section of the ice shelf, the ice flow has very small flow-direction accelerations. Only near the edge does the ice flow accelerate toward the ocean; then the vertical velocity profile in Fig. 7 becomes clear. Moreover, in the central thick ice area, there is a stagnant region with ice flow speeds less than 50 m/yr. The small ice velocities for the central area primarily are a result of the relatively large ice thickness. The small dynamic mass balance for the interior of the ice shelf explains why ocean melting mostly balances the precipitation. Consequently, the ice shelf usually is called a buttressing ice shelf, which also prevents direct ocean/ice interaction for inland ice. With the massive rate of basal ablation of the ice shelf by underlying ocean water [33], it is uncertain if ice shelves can maintain near balance in a warming climate.

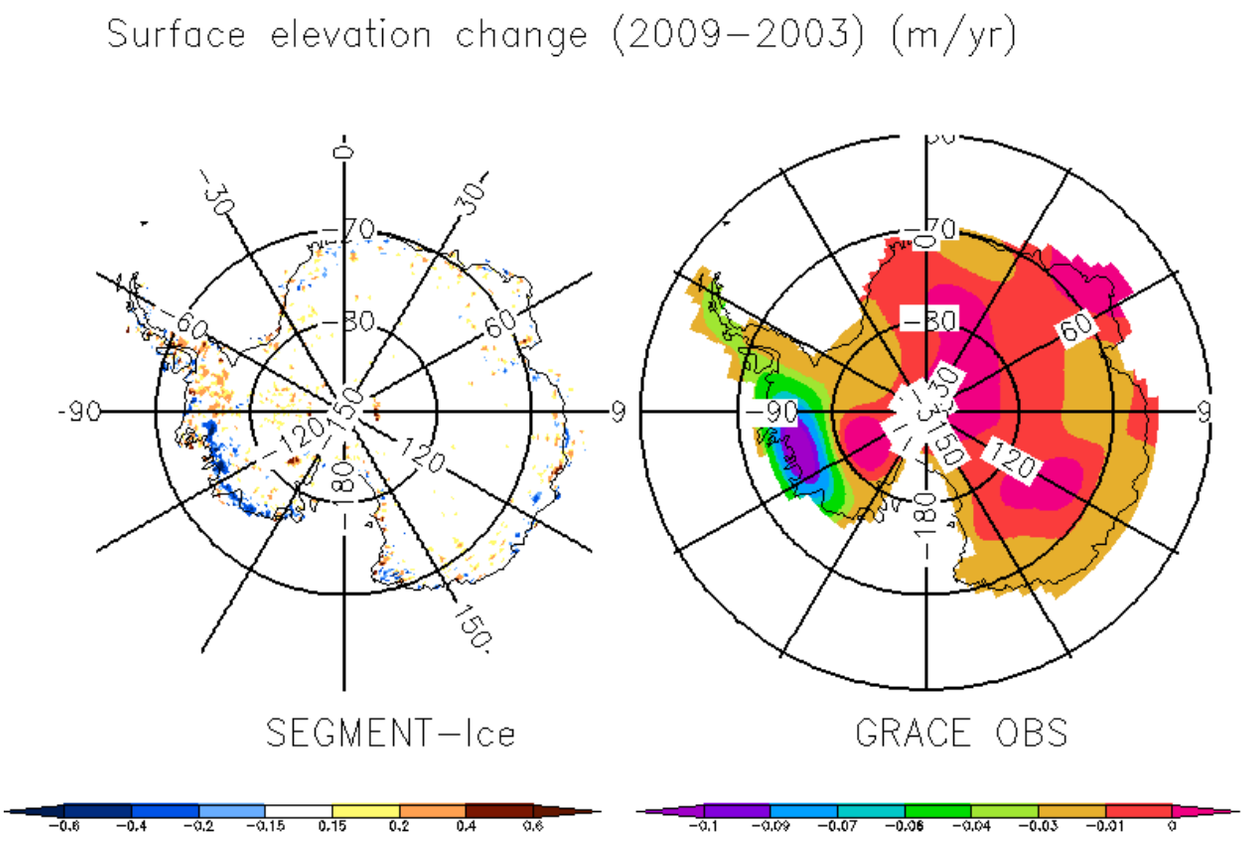

Figure 8. Left panel is the SEGMENT-Ice model simulated surface elevation change between 2003 and 2009 in m/yr (measured as the difference 2009 minus 2003). The right panel is that obtained from the GRACE observations for the same period.

Figure 8 compares the SEGMENT-Ice simulations with the Gravity Recovery and Climate Experiment (GRACE) measurements. The observed mass loss rate for land-based ice in the Antarctica is ~193 km^3/year during 2003-2009. Figure 8 (left panel) shows the SEGMENT-Ice simulated geographic distributions of rates of surface elevation changes over Antarctica between 2003 and 2009 (m/yr equivalent water thickness change). Figure 8 (right panel) is the GRACE observations of ice mass change rate over the same period. The post-glacial rebound (PGR) is removed using the method of [31]. A de-correlation filter and a 300-km Gaussian smoothing have been applied to the raw data. Note that the model provides more details than the GRACE observations. That part of West Antarctica facing the Amundsen Sea has a systematic mass loss (>0.6 m/yr in model and the smoothed GRACE observations show >0.1 m/yr reduction in surface elevation) during the five-year period. As a whole, the WAIS is losing mass, but the ridges are gaining very slightly during the five-year observation period, a feature captured by the model, but not well differentiated by the coarse resolution of the GRACE measurements.

To access the credibility of the SEGMENT-Ice mass loss rate estimates of Fig. 8 (left panel), the NCEP/NCAR reanalysis data was merged with atmospheric forcing from CGCMs for 1948-2009. Coupled ocean-atmospheric climate models have difficulty in reproducing the observed interannual and decadal climate variations and cannot be used as climate forcing for

http://dx.doi.org/10.5772/55529

SEGMENT-Ice model validation against observations on those time scales. More realistic climate forcing is provided by the NCEP/NCAR reanalyses [34]. Reanalyses are used by climate researchers as surrogates for real observations on large spatial scales. As mentioned above, Figure 8 (left panel) shows the surface elevation changes of the AIS between 2003 and 2009. Currently, the mass loss in Antarctica is dominated by ice flow acceleration in parts of West Antarctica. In this respect, SEGMENT-Ice simulated mass loss rates are close to GRACE measurements, as well as revealing details that GRACE, limited by its horizontal resolution, cannot identify. For example, the model simulations show clearly it is the peripheral sectors of WAIS that have lost mass most significantly, due to ice dynamics. In addition to changes in surface mass balance, these sectors also have suffered enhanced submarine melting and a consequent grounding line retreat and acceleration. In contrast, the Whitmoor Mountains gain mass from increased snow precipitation. Shelf dynamics likely play a role because peripheral regions that shows significant (>10 cm/yr) mass losses are mostly near major ice shelves: e.g. the Amery and West Ice shelves and the fringing shelves around Dronning Maud Land in East Antarctica. Examining present ice-water geometry near the calving front of the Ross Ice Shelf indicates that, for the next systematic tabular calving to occur, the ice surface elevation must be lower by ~20 m. This indicates that the backward stress it provides to the inland ice is lower than its 'climatological' value. Without considering ocean and atmospheric warming, buttressing gradually will be restored in the next two decades. Despite the very different resolutions, (the model has a 5-km resolution), the overall mass loss rate of ~180 km^3/yr is close to GRACE observations. From Eq. (1), total ice mass loss is comprised of ice flow divergence and boundary mass input/loss (During the reference period (1900-1920) for ice mass loss from climate warming, it is assumed that dynamic mass loss almost equals surface mass balance, with the difference being the interglacial residual trend. With this assumption, variation of modelled total ice mass is a function of anthropogenic climate warming, not past climate. The spread in future scenario, different model runs are also more representative of changes of atmospheric conditions as climate warms, minimizing uncertainty associated with their detailed parameterizations in atmospheric/oceanic physics. Thus, the following best represents the climate warming effect on the AIS total mass balance. Surface elevation changes of AIS between 2000 and 2060 are examined further under the CCSM3 A1B scenario. In general, the peripheral areas are losing ice from climate warming. For the Antarctica Peninsula, a 1 m/yr lowering of the surface elevation is sustainable (Fig. 9); loses more mass because of higher surface air temperatures and summer surface melt. Precipitation is highest but the increase does not compensate for mass loss from extra melting. Because of the higher temperatures, ice flow speeds also are higher. This sector has the most rapid change over the widest area and the greatest impact on total ice mass loss. Some interior regions have significant ice surface elevation increases, e.g. 0.2m/yr upstream of the Ross Ice Shelf. Small-scale elevation increase/decrease pairs in the interior of the ice sheet may persist as they can change sign, likely due to snowfall fluctuations. There are signals from the dynamic flow response to a warming climate. Near the Foundation Ice Stream, there is significant mass gain in the 21st Century from ice flow convergence. The meandering banded patterns of mass loss, most significant near the coast but reaching several hundred kilometres inland, are persistent features of the dynamic response of ice flow to a warming climate.

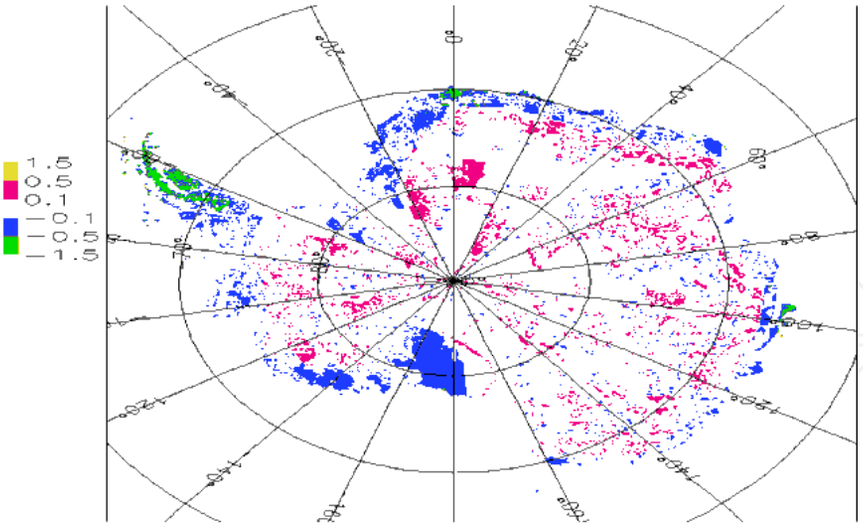

Figure 9. SEGMENT-Ice simulated geographic distributions of rates of surface elevation changes between 2000 and 2060 (m/yr). Peripheral areas and the AP lose mass most significantly. Upper streams of the Foundation Glacier gain mass from increased snowfall. The inland alternative, tributary patterns of mass loss and gain arise from dynamic response to climate warming, corresponding to ice flow convergence/ divergence pattern

The marine based ice sector of West Antarctica, confined by Marie Byrd Land, Siple coast and the Whitmoor Mountains, discharge ice primarily to the Ross Ice Shelf. As the climate warms, increased snowfall partially compensates the effect of flow divergence for the marine based ice. The increases in ocean temperature are ~ 0.2 K for the surrounding oceans, and the increased erosion of the ice shelves from oceans are ~ 1m/yr. The elevation increases caused by net snow accumulation are less than 0.1 m/yr. Horizontal spreading within an ice-shelf is laterally accelerating. This would be a thinning effect for local ice thickness if the shelf has uniform thickness. Interestingly, the thickness profile already has adjusted to this flow pattern and is thinner ocean-ward. Thus, the ice shelf resembles a stream-tube. The thickness change of ice from convergence/divergence is minimal. Consequently, the restoring of the buttressing stress is slowed by oceanic erosion of the shelf thickness, and the discharging of marine-based ice is enhanced. The marine based sector of ice mass loss, which actually is land ice with base elevations below sea level, also has a SLR contribution. There is another mechanism from oceanic warming which causes a reduction in the buttressing effect. Due to the small vertical shear in the flow profile, the calving front is slanted forward (the semi-mushroom shaped structure, right tip-end of Fig. 7c). This means that the ocean-ward section is not fully supported by the buoyancy, and extra weight is placed on the section toward the grounding line, causing this section to be submerged more than is necessary to support its own weight. This trend continues until a critical point is reached and a tabular calving event occurs. At this point, the calved iceberg lowers the weight centre and the remaining ice shelf rebounds upward (less submerged in the water). With this cycle, the buttressing effect fluctuates. Ocean water has a pole-ward temperature gradient. For the fringing ice shelves of Antarctica, the ocean temperature at the calving front is warmer than around the grounding line. If this gradient is larger than $0.0007\nabla H$ °C/m, where H is the shelf ice thickness, ocean melt also contributes to tabular calving and to a reduced buttressing effect for the inland ice.

http://dx.doi.org/10.5772/55529

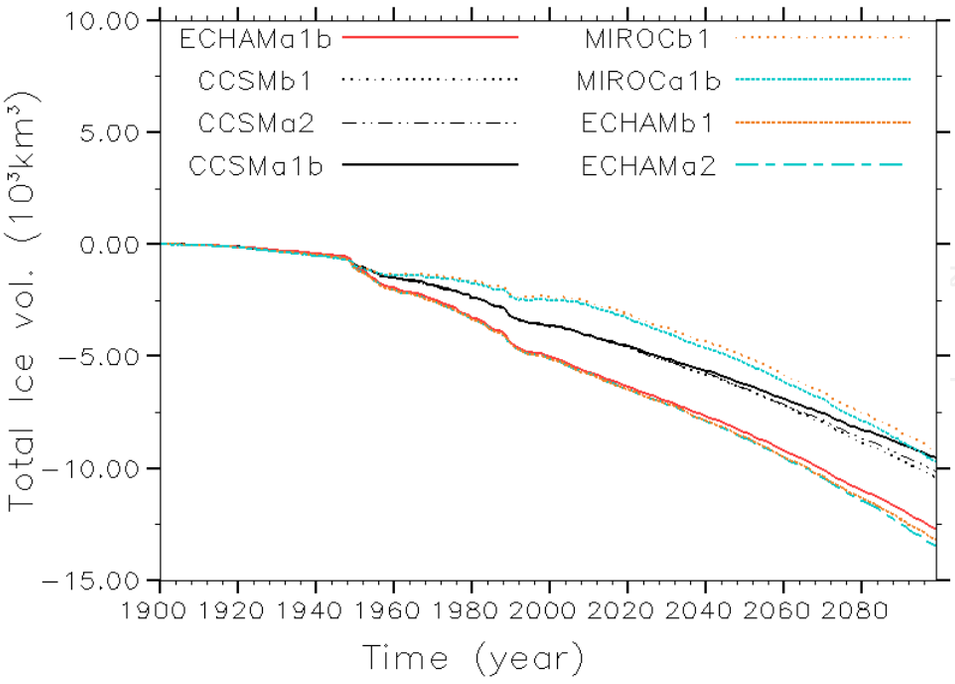

Figure 10. Total ice volume changes obtained by forcing SEGMENT-Ice with atmospheric parameters from three CGCMs, under the IPCC A1B, B1 and A2 scenarios. The 1948-2008 period uses NCEP/NCAR reanalysis data (identical across models and scenarios). Clearly, the inter-model differences are larger than the inter-scenario differences. However, the rates of decrease are similar between the models.

The above results are only for CCSM3 under the SRES A1B scenario. Atmospheric and oceanic forcing parameters were used from two other CGCMs: the MIROC-hires and ECHAM/MPI-AM. These are independently developed models. With 1948-2009 replaced with reanalysis atmospheric forcing, total mass loss rates are different between the CGCMs (Fig. 10). Only the CCSM3 mass loss rates are close to GRACE measurements. The lower MIROC-hires loss rate is due to its warm global air temperature bias of about 2 degrees above observations. Thus, reanalysed temperature field, compared to the MIROC-hires 1900-1920 reference period, is too low and there is less ice melting around the AP, resulting in a slower mass decrease than reality. Systematic biases in ECHAM/MPI-AM temperature and precipitation are lower. Outside the period 1948-2009, mass loss rates are similar among the CGCMs. Using the 1900-1920 reference periods of each climate model, there are large inter-model and inter-scenario similarities in mass loss rates, with a magnitude of spread less than 10% of the absolute decrease, compared to the 1900 level, up to year 2100. Compared with other mountainous regions, the AIS surface is flat, with the steepest slope less than 14 degrees in the 5-km SeaRISE topography data set. This poses less of a challenge for atmospheric components of the CGCMs, and all three models have similar weather patterns over the entire AIS. Region-specific biases thus are not of concern.

The high inter-model and inter-scenario consistency adds confidence in the quantification of future sea level change contributions from the AIS. As ice temperature increases, the viscosity decreases and ice flow increases. Ice flow divergences also increase, resulting in a more significant mass loss. The sensitivity of the AIS ice flow to a warming climate likely results

from three positive feedback mechanisms, described by [35]; most notably the positive feedback between granular basal slip and the ice flow. The coastal sectors are increasingly coupled with the interior regions along the preferred channels of ice streams. These ice streams form because of the slow turnover time of the ice that changed its rheological property under gravity on slopped surfaces. The ice along steeper slopes creeps progressively faster, forming an ice stream. Downstream towards the ocean there is granular material formation and accumulation. A warming climate enhances ice deformation and positive feedbacks are triggered among ice flow, granular material accumulation, and reduced resistance to further deformation. These processes provide an explanation for the accelerated rate of mass loss in the 21st century. At the flanks of ice streams, large horizontal transverse stresses create crevasses. The crevasses, when advected downstream to ice shelves, act as seeding cracks that enhance tabular calving.

2.3. Summary

Current CGCMs are not coupled with sophisticated land-ice models, so the uncertainty of the GrIS melting contribution to SLR is large. This study projects the eustatic SLR contribution from GrIS using a new ice dynamics model, SEGMENT-Ice [15]. Forced by CCSM3 atmospheric parameters, the SEGMENT-ice model is integrated for 200 years (1900-2100). The near-surface ice temperature increases for most of the GrIS (Fig. 5, [16]). The greatest warming of over 3°C by 2100, under SRES B1, corresponds to high precipitation areas in a band along the 2000 m GrIS elevation contour. The ice warming decreases inland and reaches a minimum (~0.5°C for SRES B1) at the Summit. As ice viscosity decreases with increasing temperature, the warming pattern adds extra divergence to the original flow field. This ice discharge process probably scales in proportion to surface temperature changes. The average mass loss rate projected by SEGMENT-Ice over the latter half of the 21st century is equivalent to ~0.64mm/year global mean SLR, which is significantly greater than the IPCC AR4 estimates. The lower limits of the IPCC AR4 estimates (0.01 m, under A1B) therefore should be increased to ~30 mm by 2100, with 95% confidence, assuming other sea level change contributors remain unchanged. To investigate the spatial distribution of the melt water, ice model simulated GrIS mass loss time series are used as input to climate models. The SLR is geographically non-uniform, reaching 1.69 mm/year for the northeast coastal United States, being amplified by a weaker meridional overturning circulation in the Atlantic Ocean. In other oceans, e.g. the Pacific and southern oceans, projected changes are far smaller. Both steric effects and contributions from melting mountain glaciers flatten with warming [36], but the GrIS melting contribution accelerates before declining surface area imposes a limit; this is highly unlikely in the 21st Century. For the AIS, the sensitive and uncertain basal granular material properties are retrieved from InSAR observed surface ice velocities (e.g., using a best fit of model simulated surface velocity and observed surface velocity as retrieval criteria). With improved granular rheological parameterizations, SEGMENT-Ice is driven by atmospheric parameters provided by CGCMs to project of future mass shed from the AIS. There is a high level of inter-model and inter-scenario consistency, with all indicating that the mass loss rate increases with time, and is expected to reach ~220 km^3/yr by 2100. Although they have no direct sea level change contribution, ice shelves are integral components of the AIS. Periodic calving, as a

http://dx.doi.org/10.5772/55529

normal ablation process, releases tabular icebergs to maintain a dynamic balance of the AIS. In a warming future climate, increased air and ocean temperatures thin the ice shelves by surface erosion, but also they increase the vertical shear near the ice shelf front and cause more frequent tabular calving. Direct erosional ice shelf thinning and ice sheet rebounding, after calving, both signify reduced buttressing effects that lead to further increases in the inland ice mass loss rate. Of note is that when the SLRs from the GrIS and the AIS are combined, the average SLR contribution is +2 mm/yr over the 21st Century.

3. Sea level rise from basin volume change

In Section 2, sea level change from increased input from cryosphere was discussed. Sea levels can change even without an increase of seawater total volume, for example in cases of basin volume changes. There are many causes of basin volume changes, e.g. glacial rebound (PGR), underwater earthquake deformation of the sea bed, and landslides that shed significant amounts of debris into open waters, often also from earthquakes. In the next subsection, a previously overlooked mechanism that may cause faster sea level changes than melting of the cryosphere is discussed. It also is affected by a rapidly changing climate.

3.1. West Antarctica Ice Sheet's possible future disintegration may cause landslides

As it is the largest potential contributor to SLR, quantifying the AIS total mass balance is important to the global hydrological cycle and fragile polar ecosystem consequences. The AIS, especially the West Antarctica Ice Sheet (WAIS), has been extensively studied [37-40]. Much grounded ice in west Antarctica lies on a bed that decreases inland and extends well below sea level (Fig. 11). This bathymetry makes WAIS subject to marine-ice sheet runaway instability [40]. Complete WAIS melting requires ~10^{21} J, equivalent to 30,0000 Pinatubo-size volcanoes, which cannot be provided under natural conditions on a century time frame.

Marine-based ice sheets have SLR contributions without melting completely, as they need only be partially afloat, which is possible if the basal melt water is connected to the oceans. At present, the WAIS stability results from the presence of buttressing ice shelves. Because much of the WAIS inland ice has basal melting, the gravitational driving stress cannot be balanced locally. Ice-shelves have flat (upper/sub-aerial) surface elevations and need little resistive stress to maintain balance (except near the tip-end). The hydrostatic pressure from the submerged portion of ice shelves provides the primary resistive stresses for the neighbouring coastal land ice, to balance gravitational driving stress arising from uneven surface topography. Warming from underneath the marine-based ice sheet, particularly that affecting ice-shelf viability could release this potentially fragile stability and lead to accelerated creeping of the WAIS. Ice is brittle at higher strain rates, especially under tension, because its melting point diffusivity is around 10^{-15} m^2/s, which is much lower than the values of ~10^{-11} m^2/s for elemental metals. Accelerated creeping thus implies likely breaking up of the WAIS. At the same time, after ice shelves are removed, the pathway for seawater to erode marine based ice sheets becomes open.

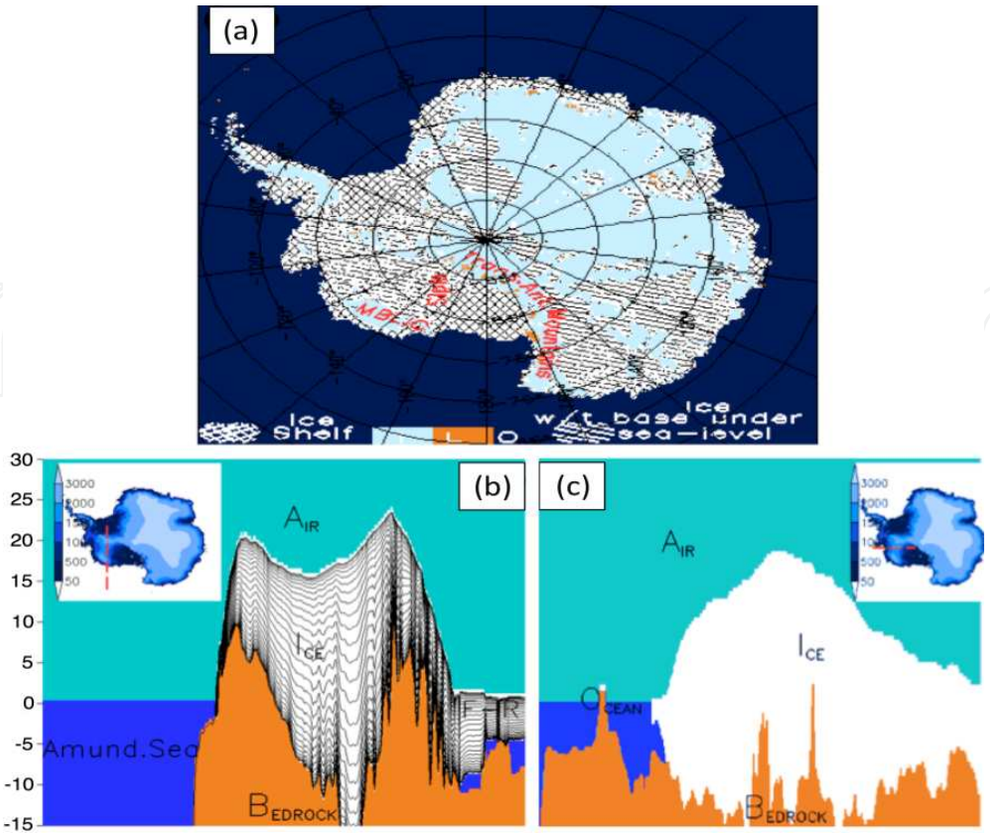

Figure 11. a) Antarctica land-ice-ocean mask based on SeaRISE 5-km resolution digital elevation, ice thickness and bedrock elevation data. Colour shaded white is ice, yellow (brown) is bare ground (L), and blue is ocean. The ice shelves are cross-hatched; land-ice with base under sea level (marine based) is hatched. West Antarctica has more complex ice-water-bedrock configurations than the rest of Antarctica. The WAIS is confined by the Transantarctica Mountains and 40 °W longitude. The Peninsula has a limited ice volume (<3.3×10^4 Gt) compared with land-based ice of WAIS (~2.8 ×10^6 Gt). Panels (b) and (c) are the West Antarctica land-ice-ocean mask from SeaRISE 5-km resolution digital elevation, ice thickness and bedrock elevation data. Colour shading is ice (white), bedrock (yellow, brown) and blue (ocean). Panel (b) is a cross-section along the F-R shelf/Amundsen direction (inset; red dashed line). Panel (c) is along the Siple coast direction (inset; red line). In a future warming climate, ocean waters likely enter the WAIS through the Siple coast pathway. The extensive troughs (if ice is removed) can reach depths > 2 km. Colour-shading in insets is surface elevation over the AIS. Marie Byrd Land Ice Cap (MBLIC) and the Whitmoor Mountains ("WM") are labeled.

With the breaking of ice, sectors which have thicknesses below $h_b \rho_w / \rho_i$, where h_b is the bedrock elevation, can float and therefore make an actual contribution to SLR.

Warming factors include drastic increases of geothermal activity from large volcanic eruptions. Although of low probability, they cannot be discarded because of feasibly high impact over a short time period. [42] identified a possible recent active volcano under Ice Stream B (now the Whillans Ice Stream) on the WAIS. Possibly, sub-glacial volcanism could accelerate an existing grounding line retreat, instigating disintegration of the WAIS.

More important is the gradual but widespread oceanic and atmospheric warming driven by anthropogenic greenhouse effects, which is assumed to be salient in the upcoming century (see IPCC AR4, 2007). The likelihood and exact timing of a WAIS collapse are as yet unknown and this study re-examines the SLR resulting from a WAIS collapse, a possibility initially proposed

http://dx.doi.org/10.5772/55529

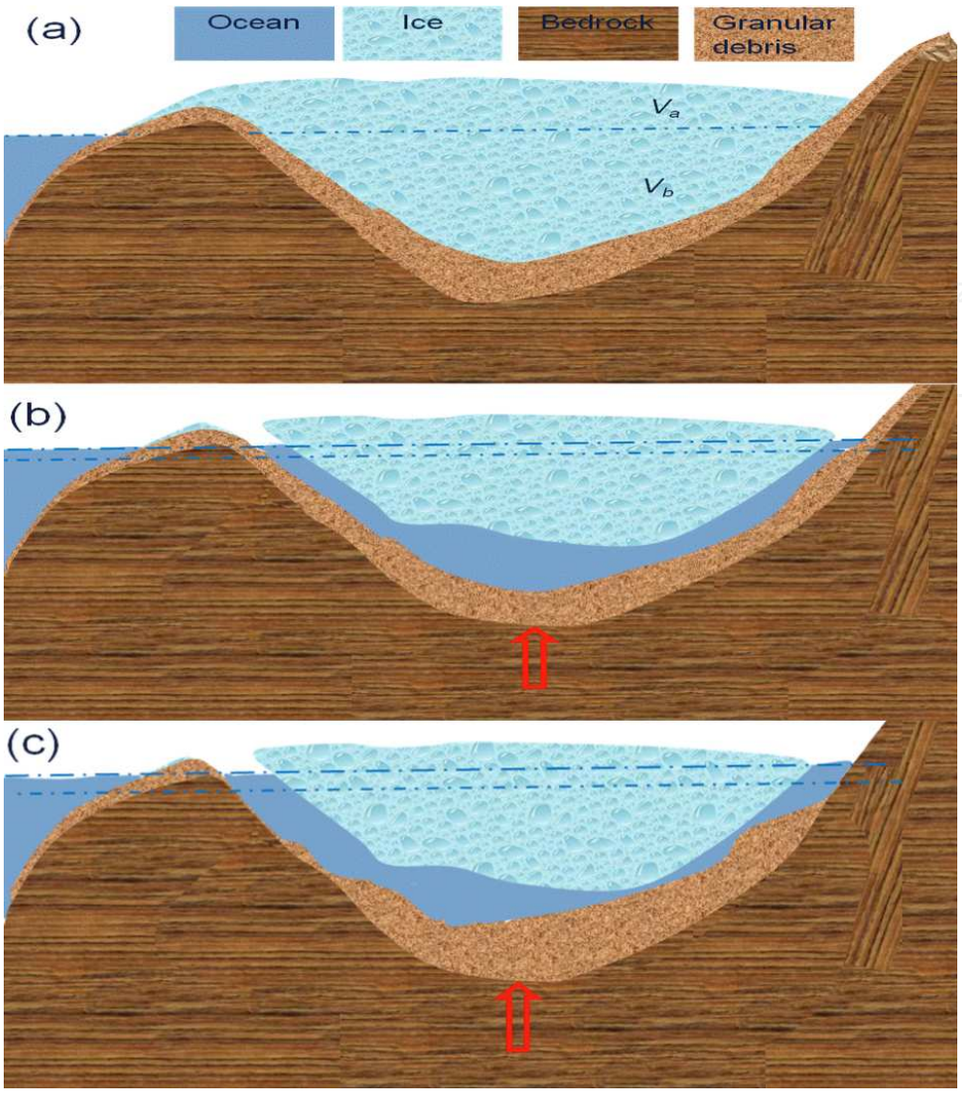

Figure 12. The eustatic sea level rise (SLR) is shown after disintegration of the WAIS. Panel (a) is the ice-bedrock configuration before the WAIS disintegration. As the WAIS is disintegrated, the vacant below future sea level will be occupied by seawater. The net contribution is the water equivalent of the integrated ice adjusted to account for the volume below sea level (V_b) and for the postglacial rebound of the bedrock (*red arrow*, V_r). Panel (b) is the SLR under this hypothesis.

in [37]. The estimate of [37] is based on the following reasoning, and is illustrated in the sequence of Figs.12a-c, below. As the WAIS disintegrates, the resulting vacancy, which is the space below sea level that was filled by solid ice, then will be occupied by seawater. The net amount of the contribution is the water equivalent of the disintegrated ice, adjusted to account for the volume below sea level (V_b), and for the postglacial rebound of the bedrock (V_r).

Fig. 12b, above, illustrates the SLR under this theory. The SLR can be expressed as $\frac{V_a \rho_i}{\rho_w} + V_b \frac{\rho_i - \rho_w}{\rho_w} + V_r$, where V_a is the ice volume above sea level. This expression slightly relaxes the free-board condition of [37], which assumed that when the summation of the first two terms is positive, the WAIS is floatable. A slight surface elevation decrease, from either negative total

surface mass balance or accelerated discharge toward the ice-shelves when oceanic interactions make the ice-shelf thinner, and hence reduce the buttressing effects, will set a significant portion of WAIS afloat. Recently, [39] made a major advance on the original estimate of [37] by using non-static bathymetry from a sophisticated Earth model, and concluded that only a portion of WAIS satisfies the marine ice sheet instability hypothesis, and can become afloat. Inevitably, after the removal of the WAIS, landslides, primarily from Marie Byrd Land, will further change the basin shape, as shown in panel (c). In principle, only the debris situated originally above sea level has a SLR contribution after sliding down-slope to locations below sea level (V_g). The SLR then becomes $(V_a + V_b)\frac{\rho_i}{\rho_w} - V_b + V_r + V_g$. These studies, however, did not take into account the fact that ice overlaying bedrock is an ideal configuration for rock erosion and the production of a large amount of granular material, especially beneath Marie Byrd Land and the Siple coast). Loading of thick ice above slopes reduces landslide occurrence because of the large confining pressure and because granular debris is effectively cemented by ice crystals. Inevitably, after the removal of the WAIS, landslides will further change the basin shape (Fig. 12c) on time scales much shorter than the basin rebound. In principle, only the debris that is originally above sea level has a SLR contribution when it slides to locations below sea level (R. Alley, Personal Communication 2011). V_g is estimated using the SEGMENT-Landslide model [1], driven by meteorological parameters provided by coupled climate models.

3.2. Data and methods

SEGMENT-Landslide accounts explicitly for soil mechanics, vegetation transpiration and root mechanical reinforcement, and relevant hydrological processes. It considers non-local dynamic balance of the 3D topography, soil thickness profile, basal conditions, and vegetation coverage [15] to project the driving and resistive forces. It describes flow fields and dynamic evolution of thickness profiles of the medium. SEGMENT-Landslide monitoring and predicts landslides and their ecosystem implications. Applications to the polar environment of the WAIS pose fewer challenges for SEGMENT-Landslide because vegetation is not involved. In addition, rainfall morphology is not a concern because solid precipitation dominates. Monthly mean atmospheric forcing parameters suffice for driving the temperature solver, which estimates frozen soil mechanical properties. Three independent CGCMs (MPI-ECHAM, NCAR CCSM3 and MIROC3.2-hires, (http://www-pcmdi.llnl.gov/ipcc/about_ipcc.php) have relatively fine resolution and provide all atmospheric parameters required by SEGMENT-Landslide. Sub-glacial particle properties of WAIS are specified from boreholes and seismic studies (e.g. [43]). The rocks are mostly volcanic and the basalt clasts are of sizes ~10 cm. Loose, ice-cemented volcanic debris also is widespread around Mt Waesche (77°S, 130°W) and the northern Antarctica Peninsula and its constituent blocks. In assigning granular particle sizes, geothermal patterns also are referenced because repeated phase changes at the interface of ice/rock arguably are the most efficient means of erosion and reducing the granular particle sizes. A high-resolution digital elevation map (DEM) is a key input for slope stability analyses.

The SeaRISE project (http://websrv.cs.umt.edu/isis/index.php) provides surface DEM at 5 km horizontal resolution on a South Polar Stereographic projection. The actual sphere resolution

http://dx.doi.org/10.5772/55529

is higher at the WAIS, but coarser than 1000 m. Radarsat-1 SAR sensor via MAMM, as a by-product, provides slope information at 200 m resolution. A 200 m resolution surface DEM is obtained by combining SeaRISE and MAMM data. Assuming no major geothermal disturbance from volcanic eruptions, SEGMENT-Landslide simulations indicate that except for very limited northern areas, such as Deception island, where avalanches are likely and involve limited mass redistribution ($<10^5$ m^3) the present WAIS is stable. In addition to mechanical properties such as particle size, porosity, bulk density, cohesion and repose angle, the granular material thickness is critical in determining the landslide magnitudes. Granular thickness on slopes underneath the present WAIS is inversely retrieved using SEGMENT-Ice [16], constrained by the goodness of fit between model simulated and observed surface ice velocity, over the entire AIS. Figure 13 is the distribution of the estimated granular material thickness over West Antarctica. This is the initial sliding material thickness.

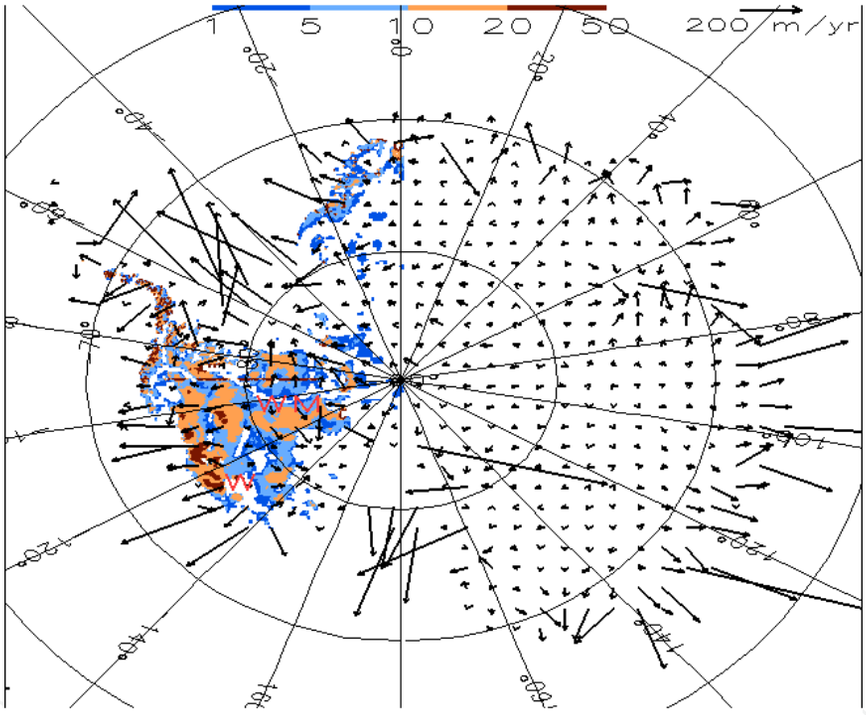

Figure 13. SEGMENT-Ice simulated surface velocities (vector arrows) over the AIS, and retrieved granular material depth under the overlain ice (colour shading, in metres) over the WAIS. The top portion of Mountain Waesche ("W") and the ridge of Whitmoor Mountains ("WM") have shallow debris accumulations (<1.0 m).

Magnitudes of surface ice velocities are sensitive to the thickness of the basal granular material. Based on this sensitivity relationship, repeated projections of the ice model are performed with present ice geometry and ice temperature profiles, but with automatically varying granular layer thickness, to best fit the observed surface ice velocities. Observed ice velocities are obtained from MAMM as described in [32]. As the 7 regional composite of MAMM do not cover the entire AIS (because of the "polar hole"), the metric summation is only over regions with MAMM observations. Upon convergence, the overall agreement between modelled and observed velocities is high, with correlation coefficients of 0.92 for direction and 0.90 for

magnitude, respectively. Modelling experiments were carried out to estimate possible landslides contributions to SLR as the WAIS disintegrates. The ice-bedrock configuration of SeaRISE is the same as [45], except they did not consider the contribution of landslides, but all other factors were included. Their estimate is the most recent for the SLR contribution of the WAIS. The SLR contribution is estimated from the following method. SEGMENT-Landslide uses a terrain following coordinate system, the sigma coordinate system. Assuming the sliding material is incompressible, a vertical integration of the incompressible continuity equation, assuming no external sources of granular material, gives:

$$\frac{\partial h}{\partial t} = - \frac{1}{R\cos\phi}\int_0^1 \left(\frac{\partial u}{\partial \theta} + \frac{\partial v\cos\phi}{\partial \phi}\right) H ds - \frac{u_s}{R\cos\phi}\frac{\partial h}{\partial \theta} - \frac{v_s}{R}\frac{\partial h}{\partial \theta} - w_b \quad (10)$$

Equation (10) is similar to Equation (1) without the surface source term. Equation (10) diagnoses the temporal evolution of the surface elevation and is the sliding material's thickness because bedrock is assumed unchanged over the time scale of several hundred years. It varies because of velocity fields and boundary sources. Changes in surface elevation multiplied by grid area give the mass loss volume for that grid. The total SLR contribution is the sum over all grids with basal elevations above sea level.

3.3. Results and discussion

Figure 14 shows the model-projected surface elevation changes of the bare slopes and, for areas under seawater, the bedrock elevation changes. Landslides can cause some areas to accumulate more than 200 m of sliding material. The most significant regions for volcanic rock and silt debris accumulation are close to Siple coast. However, the source region of the sliding material is primarily the southeast facing slopes of Marie Byrd Land, which contribute ~86% of the accumulated sliding material. Contributions from the Whitmoor Mountains are relatively small (<10%), due primarily to existing granular material on the slopes (Fig. 14). The total volume of the scars on the slopes at elevations above sea level, or equivalently the reduction of the basin volume of the below sea level areas is 3220 km^3, that is ~0.902 cm eustatic SLR. Although small compared with the ~3.3 m eustatic SLR from the collapsed WAIS, it is added to the eustatic sea level with a very short time delay, closely following the ice disintegration. If the fast scenario of [39] is realised, the economic cost to coastally based global cities from the additional 0.902 cm is not a simple linear addition to the 3.3 m SLR.

In contrast, the rebound contribution of the basin bottom takes over 10,000 years, providing a long period for human adaptation and mitigation measures. Landslides considered here primarily are associated with granular material as the ice bonds melt and when the solid ice loading is removed. The two most frequent triggering mechanisms for large-scale landslides, rainstorms and earthquakes, both are negligible. The former is apparent from the year round low air temperatures over the WAIS. Earthquakes are rare in Antarctica, as the Antarctica plate now has only a small portion associated with subduction and is bounded by constructive and conservative margins. Thus, the estimates from this study are expected to be highly representative of the SLR caused by the disintegration of the WAIS. The scarp sizes and the maximum sliding speeds both are sensitive to WAIS

http://dx.doi.org/10.5772/55529

disintegration scenarios, but the total volume of the sliding material involved is a conservative property that is insensitive to fast/slow scenarios [39].

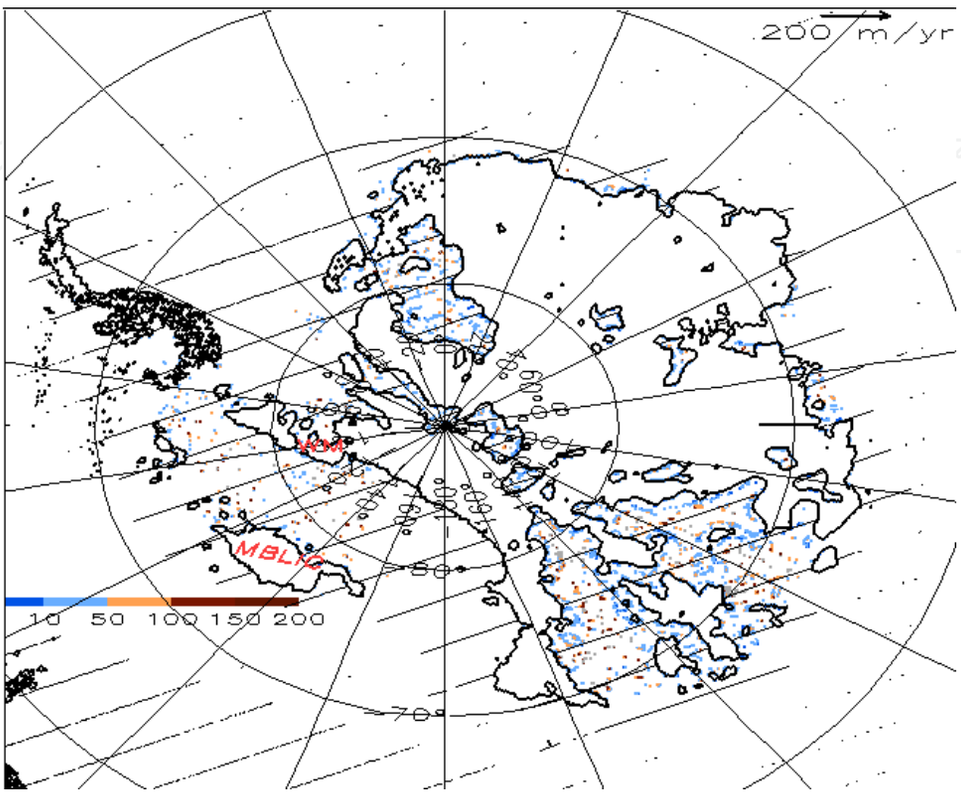

Figure 14. Areas with bedrock elevation increases over 5 m, from landslides accompanying de-glaciation of the WAIS. They are colour shaded (m). The bedrock zero elevation contour lines are shown and areas with bedrock elevations below sea level are hatched. Landslide scars are prominent on the slopes, with localized pairs of elevation increase and decrease. However, regions accumulating most of the sliding material (>5 m depth) are almost below sea level. Marie Byrd Land Ice Cap (MBLIC) and Whitmoor Mountains (WM) are labelled for reference. The southeast facing slopes of MBLIC contribute most of the sliding material.

The model predictions confirm that melting of the WAIS is not possible in the upcoming centuries, but breaking and partial floating of ice is possible, provided the sea water could find pathways to the bottom of ice sectors, which have basal elevations below sea level and low free-board potential. Then the WAIS might disintegrate in a future warming climate. In this modelling study, the potential contribution to eustatic SLR from a collapse of the WAIS is reassessed, and that previous assessments have overlooked the WAIS as a potential major contributor through slope instability if bolstering ice is removed. Overloading ice has a buttressing effect on slope movements in the same way that ice shelves hinder the flow of non-floating coastal ice. Landslide modelling provides estimates of ~9 mm eustatic SLR contribution from WAIS landslides. Note that changes in sea water volumes caused by melting of the cryosphere are persistent but slow processes. Comparatively, the changes of basin sizes caused by landslide filling, from climate warming or from geo-hazards such as tsunamis, are likely to be far quicker, although the SLR contribution likely will be smaller.

4. Coastal line erosion because of sea level change

Shorelines are unique features and are referred to as "Geo-Indicators" in [44]. They never have had long-term positions. Shoreline change has a direct impact on communities, property, industrial and recreational facilities, and species living on both sides of the shoreline. [45] has shown that shoreline change is increasingly affected by climate warming. The relative abundance of glaciers in the current climate suggests that a large SLR is possible from the current cryosphere. As one critical factor contributing to shoreline erosion, the SLR threatens many coastal ecosystems (e.g. [46]). Climate change impacts also include possible increases of sea-surface temperatures and greater variability in patterns of rainfall and runoff [47]. Altered wind patterns and possible changes to wave climate and frequency, storms intensity and duration (see [48]) all accelerate coastal erosion and increase inundation of low-lying areas, and cause saline intrusion into coastal waterways. To predict shoreline changes, simply mapping the bathymetry and coastal surface elevation clearly is inadequate as shoreline susceptibility depends on coastal geological composition, in addition to coastal slope, and are estimated in [49].

The claim that water depth is invariant is appropriate for sandy coasts, has been verified by a number of studies [50]. SLR is accompanied by significant changes in wave heights and tidal ranges. Thus, the relative SLR, wave and tidal changes all should be input to coastal erosion models. This requires that the models in [49] need to incorporate more processes that affect shoreline erosion, because the actual geological features of the coasts are highly complex. Model verifications are now possible because recent advances in satellite imaging and LiDAR remote sensing as described in [51] allow a more cost-effective mapping of shorelines at multiple scales.

5. Conclusions

A natural hazard of increasing concern is a global (eustatic) sea level rise (SLR). Estimating the size and rate of increase of SLR is an urgent observational and scientific challenge. The current cryosphere has the capacity to contribute to the eustatic SLR. Many regions of the Earth, especially low-lying islands and some coastlines, are vulnerable to present SLR. SLR can result from volume variations in ocean basin In this chapter it is shown that a multi-disciplinary modelling approach (Section 1) is needed to investigate the SLR contribution from the two largest ice sheets in the cryosphere: the Greenland Ice Sheet (GrIS) and the Antarctic Ice Sheet (AIS), in a warming 21st Century climate. It was found that the water discharge from the two ice sheets both would increase as the climate warms. For the GrIS, because it discharges water into the northern branch of the Gulf Stream, there are regional manifestations of SLR. The AIS, unlike its northern hemisphere counterpart, has numerous ice shelves that are sensitive to climate change and are of importance for total fresh water discharge into the southern Oceans.

The representation of ice shelves in the SEGMENT-Ice model is described. Using this advanced ice shelf scheme, SEGMENT-Ice simulates well the mass change rate in the past decade using

http://dx.doi.org/10.5772/55529

good quality remotely sensed verification data. A projection of the 21st Century mass loss rate is made. From the fresh water discharge alone, the combined contribution from the GrIS and the AIS is equivalent to ~2 mm/yr eustatic SLR in the second half of the 21st Century. The West Antarctic Ice Sheet also has the possibility of disintegrating in a warmer climate. If it does disintegrate, the glacial erosion will produce granular material on the slopes of the bedrock, which may slide into the ocean, causing a reduction in basin volume and a consequent SLR. The magnitude of the SLR from such a bedrock landslide is smaller but is much quicker. Finally, towards the end of the chapter, the problem of coastal erosion was examined, as it is likely to be a common consequence of SLR. The possibility that moderate or severe coastal erosion can have extremely serious socio-economic and natural environmental impacts, it seems prudent that mitigation strategies be developed and implemented as soon as practicable.

Appendix: Cryosphere terms and nomenclature

There is a wide variety of terms applicable to the cryosphere and there is a corresponding nomenclature. The major terms used in this chapter, and their meanings, are presented here in alphabetical order.

Glaciers: Glaciers are large masses of ice that flow very slowly over land. They form from the compacting and recrystalling of snow, when the snow accumulation exceeds combined melting and sublimation. They resemble very slow rivers of ice, crushing rock below, and re-shaping the terrain.

Grounding line: This is the boundary between a floating ice shelf (see below) and the grounded (resting on bedrock) ice that feeds it. When the grounding line retreats inland, water is added to the ocean and the sea level rises.

Iceberg calving: Glaciers flow, or "creep" (see below), under their own weight, and move very slowly like a viscous fluid. When the nose of a glacier reaches a coastline, pieces of the glacier break off ("calve"), producing icebergs that range in size from small to very large.

Ice creeping: Most ice flows, including glaciers, are very slow. Hence, the flows are referred to as ice creeping

Ice Sheet: An ice sheet is a very large mass of glacier ice that covers the surrounding terrain. Commonly, it is defined as having an area greater than 50,000 km^2. There are only two ice sheets at present, the Antarctic and Greenland Ice Sheets. The Antarctic Ice Shelf is by far the larger of the two and contains about 70% of the Earth's entire fresh water supply.

Ice Shelf: An ice shelf is a thick, floating platform of ice that forms where a glacier or an ice sheet flows down to a coastline and then onto the ocean surface. There are numerous ice shelves, the two largest are the Ross Ice Shelf and the Filchner-Ronne Ice Shelf, both located in Antarctica.

Multi-rheology flows: These are flows of various types of fluids. For example, water in its various phases, gas (vapour), liquid (water) and solid (ice) all are present in the cryosphere and treated by SEGMENT-Ice.

Sheet ice: Ice frozen in a relatively thin, smooth, and extensive layer on the surface of a body of water.

Stream ice: Part of an ice sheet that moves faster than the surrounding ice. Stream ice is relatively common in Antarctica and their speed depends partly on the nature of the underlying surface.

Tidewater glaciers: Glaciers that flow into the sea. As the ice moves over the sea it loses support from ground underneath and pieces break off, or calve, forming icebergs. Most tidewater glaciers calve above sea level.

Author details

Diandong Ren[1], Lance M. Leslie[2] and Mervyn J. Lynch[1]

1 Department of Imaging and Applied Physics, Curtin University, Australia

2 School of Meteorology, University of Oklahoma, USA

References

[1] Ren, D, Fu, R, Leslie, L. M, & Dickinson, R. Predicting Storm-triggered Landslides. Bulletin American Meteorological Society (2011). , 92(2), 129-139.

[2] Ren, D, Leslie, L. M, & Lynch, M. (2012). Verification of Model Simulated Mass Balance, Flow Fields and Tabular Calving Events of the Antarctic Ice Sheet against Remotely Sensed Observations. Climate Dynamics 2012; doi:s00382-012-1464-3.

[3] IPCC(2007). Climate Change 2007: The Physical Science Basis. Contribution of Working Group I to the Fourth Assessment Report of the Intergovernmental Panel on Climate Change [Solomon, S., D. Qin, M. Manning, Z. Chen, M. Marquis, K.B. Averyt, M. Tignor and H.L. Miller (eds.)]. Cambridge University Press, Cambridge, United Kingdom and New York, NY, USA, 996 pp.

[4] Zwally, H. J, Abdalati, W, Herring, T, Larson, K, Saba, J, & Steffen, K. Surface Melt-Induced Acceleration of Greenland Ice-Sheet Flow, Science (2002). , 297(5579), 218-222.

[5] Joughin, I, Das, S. B, & King, M. A. Seasonal Speedup Along the Western Flank of the Greenland Ice Sheet. Science (2008). , 320(5877), 781-783.

[6] Scambos, T. A, Bohlander, J. A, Shuman, C. A, & Skvarca, P. Glacier Acceleration and Thinning after Ice Shelf Collapse in the Larsen B Embayment, Antarctica. Geophysical Research Letters (2004). L18402.

[7] Rignot, E, Casassa, G, Gogineni, P, Krabill, W, Rivera, A, & Thomas, R. Accelerated Ice Discharge From the Antarctic Peninsula Following the Collapse of Larsen B Ice Shelf. Geophysical Research Letters (2004). L18401.

[8] Shepherd, A, Wingham, D. J, & Rignot, E. Warm Ocean is Eroding West Antarctic Ice Sheet, Geophysical Research Letters (2004). L23402.

[9] Parizek, B. R, & Alley, R. B. Implications of Increased Greenland Surface Melt Under Global-Warming Scenarios: Ice-Sheet Simulations. Quaternary Science Reviews 20004; 23(9-10) 1013-1027.

[10] Payne, A. J, Holland, P. R, Shepherd, A. P, Rutt, I. C, Jenkins, A, & Joughin, I. Numerical Modeling of Ocean-Ice Interactions Under Pine Island Bay's Ice Shelf, Journal of Geophysical Research-Oceans (2007). C10) 14.

[11] Alley, R, Anandakrishnan, S, Anderson, J, Arthern, R, Bindschadler, R, Blankenship, D, Bromwich, D, Catania, G, Csatho, B, Dalziel, I, Diehl, T, Ferraccioli, F, Holt, J, Ivins, E, Jackson, C, Jenkins, A, Joughin, I, Larter, R, Orsi, A, Parizek, B, Payne, T, Ridley, J, Stone, J, Vaughan, D, & Young, D. (2007). West Antarctic Links to Sea-Level Estimation (WALSE) Workshop. British Consulate-General Houston, DEFRA, Jackson School of Geosciences, British Antarctic Survey, March 2007., 1-3.

[12] Oppenheimer, M, Alley, R. B, Balaji, V, Clarke, G, Delworth, T, Dixon, K, Dupont, T. K, Gnandesikan, A, Hallberg, R, Holland, D, Hulbe, C. L, Jacobs, S, Johnson, J, Leetmaa, A, Levy, H, Lipscomb, W, Little, C, Marshall, S, Parizek, B. R, Payne, T, Schmidt, G, Stouffer, R, Vaughan, D. G, & Winton, M. Report of the Workshop on Ice Sheet Modeling at the NOAA Geophysical Fluid Dynamics Laboratory 8 January 2007. NOAA and Woodrow Wilson School of Public and International Affairs at Princeton University, May (2007). , 1-7.

[13] Lipscomb, W, Bindschadler, R, Bueler, E, Holland, D, Johnson, J, & Price, S. A Community Ice Sheet Model for Sea Level Prediction. EOS Transactions (2009).

[14] Rahmstorf, S. A Semi-Empirical Approach to Projecting Future Sea-Level Rise. Science (2007).

[15] Ren, D, Fu, R, Leslie, L. M, Chen, J, Wilson, C, & Karoly, D. J. The Greenland Ice Sheet Response to Transient Climate Change. Journal of Climate. (2011). , 24(13), 3469-3483.

[16] Ren, D, Fu, R, Leslie, R, Karoly, L. M, Chen, D. J, & Wilson, J. C. A Multirheology Ice Model: Formulation and Application to the Greenland Ice Sheet, Journal of Geophysical Research (2011). D05112, doi:10.1029/2010JD014855

[17] Wang, W, & Warner, R. Modelling of Anisotropic Ice Flow in Law Dome, East Antarctica. Annals of Glaciology (1999). , 29, 184-190.

[18] MacAyeal DIrregular Oscillations of the West Antarctic Ice Sheet. Nature (1992). , 359, 29-32.

[19] Alley, R, Dupont, T, Parizek, B, Anandakrishnan, S, Lawson, D, Larson, G, & Evenson, E. Outburst Flooding and Initiation of Ice-Stream Surges in Response to Climatic Cooling: A Hypothesis. Geomorphology (2005).

[20] Alley, R. Ice-Core Evidence of Abrupt Climate Changes. Proceedings National Academy of Science USA (2000). , 97(4), 1331-1334.

[21] Zwinger, T, Greve, R, Gagliardini, O, Shiraiwa, T, & Lyly, M. A Full Stokes Flow Thermo-mechanical Model for Firn and Ice Applied to Gorshkov Crater Glacier Kamchatka, Annals of Glaciology (2007). , 45-29.

[22] Thomas, R, Akins, T, Csatho, B, Fahenstock, M, Goglneni, P, Kim, C, & Sonntag, J. Mass Balance of the Greenland Ice Sheet at High Elevations. Science (2000). , 289-428.

[23] Landerer, F, Jungclaus, J, & Marotzke, J. J. Regional Dynamic and Steric Sea Level Change Response to the IPCC-A1B Scenario. Journal of Physical Oceanography (2007). , 37-296.

[24] Zwally, H, & Giovinetto, M. Balance Mass Flux and Ice Velocity Across the Equilibrium Line in Drainage Systems of Greenland. Journal of Geophysical Research (2001). , 106, 33717-33728.

[25] Dupont, T, & Alley, R. Assessment of the Importance of Ice-Shelf Buttressing to Ice-sheet Flow. Geophysical Research Letters (2005). L04503.

[26] Reeh, N. On the Calving of Ice from Floating Glaciers and Ice Shelves. Journal of Glaciology (1968). , 7(50), 215-232.

[27] Thomas, R. The Creep of Ice Shelves: Theory. Journal of Glaciology (1973). , 12(64), 45-53.

[28] Hughes, T. Theoretical Calving Rates from Glaciers Along Ice Walls Grounded in Water of Variance Depths. Journal of Glaciology (1992). , 38(128), 282-294.

[29] Scambos, T, Hulbe, C, Fahnestock, M, & Bohlander, J. The Link Between Climate Warming and Break-up of Ice Shelves in the Antarctic Peninsula. Journal of Glaciology (2006). , 46(154), 516-530.

[30] Timoshenko, S, & Gere, J. Theory of Elastic Stability. 2nd Edition., (1963). McGraw-Hill, New York, USA., 541pp.

[31] Ivins, E, & James, T. Antarctic Glacial Isostatic Adjustment: A New Assessment. Antarctic Science (2005). doi:10.1017/S0954102005002960

[32] Jezek, K. Observing the Antarctic Ice Sheet Using the RADARSAT-1 Synthetic Aperture Radar. Polar Geography (2003). , 27(3), 197-209.

[33] Bindschadler, R. Hitting the Ice Sheet Where it Hurts. Science (2006). , 311(5768), 1720-1721.

[34] Kalnay, E. and Coauthors ((1996). The NCEP/NCAR 40-Year Reanalysis Project. Bulletin American Meteorological Society 1996; , 77(3), 437-471.

[35] Ren, D, & Leslie, L. M. Three Positive Feedback Mechanisms for Ice Sheet Melting in a Warming Climate. J. Glaciology (2011). , 57(206), 1057-1066.

[36] Raper, S, & Braithwaite, R. Low Sea Level Rise Projections From Mountain Glaciers and Icecaps Under Global Warming. Nature (2006). , 439-311.

[37] Mercer, J. H. West Antarctic Ice Sheet and CO2 Greenhouse Effect. Nature (1978). , 271(5643), 321-325.

[38] Rignot, E, & Bamber, J. van den Broeke M., Davis C., Li Y., van de Berg W., van Meijgaard E. Recent Antarctic Ice Mass Loss From Radar Interferometry and Regional Climate Modelling. Nature Geosciences (2008). , 1(2), 106-110.

[39] Bamber, J. L, Gomez-dans, J, & Griggs, J. A. The Cryosphere (2009). , 3, 101-111.

[40] Joughin, I, & Alley, R. Stability of the West Antarctic Ice Sheet in a Warming World. Nature Geosciences. (2011). , 4(8), 506-513.

[41] Vaughan, D. Recent Trends in Melting Conditions on the Antarctic Peninsula and their Implications for Ice-Sheet Mass Balance and Sea Level. Arctic and Antarctic Alpine Research (2006). , 38(1), 147-152.

[42] Blankenship, D, Bell, R, Hodge, S, Brozena, J, Behrendt, J, & Finn, C. Active Volcanism Beneath the West Antarctica Ice Sheet and Implications for Ice-Sheet Stability. Nature (1993). , 361-526.

[43] Englehardt, H, Humphrey, N, Kamb, B, & Fahnestock, M. Physical Conditions at the Base of a Fast Moving Antarctica Ice Stream. Science (1990). , 248-57.

[44] Lockwood, M. NSDI Shoreline Briefing to the FGDC Coordination Group. January 7, (1997). NOAA/NOS, 29pp.

[45] Walther, G. R, Post, E, & Convey, P. Ecological Responses to Recent Climate Change. Nature (2002). , 46-389.

[46] Meehl, G. A, Washington, W. M, Collins, W. D, Arblaster, J. M, Hu, A, Buja, L. E, Strand, W. G, & Teng, H. T. How Much More Global Warming and Sea Level Rise? Science (2005). , 307(5716), 1769-1772.

[47] Patz, J. A, Campbell-lendrum, D, Holloway, T, & Foley, J. A. Impact of Regional Climate Change on Human Health. Nature (2005). , 438(7066), 310-317.

[48] Knutson, T. R. and Coauthors. Tropical Cyclones and Climate Change. Nature Geosciences (2010). , 3-157.

[49] Bruun, P. Sea Level Rise as a Cause of Shore Erosion. Journal of Waterways and Harbors Division (1962). , 88-117.

[50] Dean, R. G, & Maurmeyer, E. M. Models of Beach Profile Response. In: CRC Handbook of Coastal Processes [Komar, P.D. (ed.)]. CRC Press, (1983). Boca Raton, FL.

[51] Sampath, A, & Shan, J. Building Boundary Tracing and Regularization from Airborne LiDAR Point Clouds. Photogrammetric Engineering and Remote Sensing (2007). , 73(7), 805-812.